Heliyon 9 (2023) e18694

Contents lists available at ScienceDirect

Heliyon

journal homepage: www.cell.com/heliyon

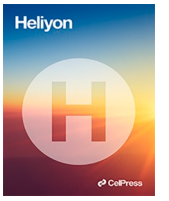

Numerical study of heat transfer, pressure drop and entropy production characteristics in inclined heat exchangers with uniform heat flux using mango bark/CO_2 nanofluid

Okwesilieze Uwadoka [a], Adekunle O. Adelaja [a,b,*], Olabode T. Olakoyejo [a], Opeyemi L. Fadipe [c], Steven Efe [d]

[a] Department of Mechanical Engineering, University of Lagos, Akoka, Lagos State, 100213, Nigeria
[b] Faculty of Engineering and the Built Environment, Durban University of Technology, PO Box 1334, Durban, 4000, South Africa
[c] Department of Industrial and Systems Engineering, Morgan State University, 1700 East Cold Spring Lane, Baltimore, MD, USA
[d] Department of Civil Engineering, Morgan State University, 1700 East Cold Spring Lane, Baltimore, MD, USA

ARTICLE INFO

Keywords:
Convective heat transfer
Gas cooling
Gravitational force
Heat transfer enhancement
Inclined flow
Mango bark/CO_2 nanofluid

ABSTRACT

For sustainable low-carbon cities, using sustainable urban energy system solutions is imperative. CO_2-based bionanofluid is one proposed energy system solution that is sustainable and environmentally friendly. This paper examines the thermal-hydraulic and entropy production properties of mango bark/CO_2 nanofluid for industrial-inclined gas cooling applications. The influence of gravitational force (in terms of tube inclination angle), volume fraction, and Reynolds number on the heat transfer, pressure drop, and entropy production of CO_2-based mango bark nanofluids in laminar flow through a circular aluminum tube are numerically studied. The bionanofluid flows through a tube with an inner radius of 2.25 mm, a length of 970.0 mm, and an initial temperature of 320.0 K. A constant heat flux of -10.0 W/m^2 is applied to the flow at its walls. The laminar flow regime with Reynolds numbers of 100, 400, 700, and 1000 are subjected to flow inclinations of $\pm 90^\circ$, $\pm 60^\circ$, $\pm 45^\circ$, $\pm 30^\circ$, and 0° and bionanofluid volume fractions of 0.5%, 1.0%, and 2.0%. Results show that $\pm 45^\circ$ tube inclination angle offers the optimal heat transfer coefficient, maximum pressure drop, and minimum total entropy production rates for $Re > 100$; however, for $Re = 100$, these occur at the inclination angle of -30° and $+60^\circ$. The pressure drop shows less sensitivity to the inclination angle; however, it offers peak values at the same inclination angles as the heat transfer coefficient for the respective Reynolds number values. The maximum thermal enhancements due to gravitational effect are 42%, 93.98%, 121.28%, and 150% for Reynolds numbers of 100, 400, 700, and 1000, respectively, while that due to nanofluid volume fraction are less than 16%.

1. Introduction

Energy is the driving force of development around the world. As advancements and breakthroughs are made in the realms of science and technology, and as the world population increases, energy consumption keeps growing per annum. The demand for air conditioners and refrigerators is rising in industrialized and developing countries, in tandem with the population and standard of

* Corresponding author. Department of Mechanical Engineering, University of Lagos, Akoka, Lagos State, 100213, Nigeria.
E-mail address: aadelaja@unilag.edu.ng (A.O. Adelaja).

https://doi.org/10.1016/j.heliyon.2023.e18694
Received 31 May 2023; Received in revised form 23 June 2023; Accepted 25 July 2023
Available online 26 July 2023

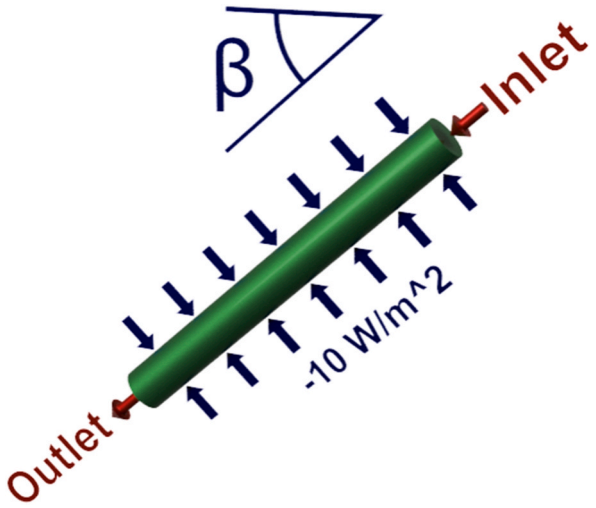

Fig. 1. Schematic diagram of simulated model.

Table 1
Thermophysical properties of various volume fraction of mango bark/CO_2 nanofluids.

Volume fraction	Thermal conductivity, k_{nf}	Density, ρ_{nf}	Heat capacity, Cp_{nf}	Viscosity, μ_{nf}
[%]	[W/m k]	[kg/m^3]	[J/kg k]	[Pa·s]
0.0ˆ	0.059	461.35	5764.81	3.45×10^{-5}
0.5	0.060	460.30	5755.60	3.58×10^{-5}
1.0	0.061	459.24	5746.15	3.74×10^{-5}
2.0	0.063	457.14	5727.13	4.12×10^{-5}

Note: ˆ 0.0% represents the properties of supercritical CO_2.

living. With exponential growth in the number of freezers and air conditioners, world energy consumption likewise rises [1]. This is a significant issue since excessive CO_2 emissions into the atmosphere from fuel consumption and power generation directly contribute to global warming and the greenhouse effect. Asides from the warming effect of CO_2, other environmental concerns are raised regarding the impact of heating, ventilation, air conditioning, and refrigeration (HVAC-R) equipment. The refrigerants used in this equipment are also harmful to the environment (Ozone layer depletion) and/or the personnel handling them (Refrigerant poisoning and flammability) [2,3]. Many researchers have suggested the use of CO_2 as the refrigerant in a vapour compression refrigeration cycle as a way to mitigate the harmful environmental effects that the aforementioned refrigerants have and to reduce the amount of CO_2 in the atmosphere [4]. This is sustainable as CO_2 is naturally occurring, and its effects on the environment are minor compared to conventional refrigerants. Further research also showed that energy efficiency in a refrigeration system could be increased by improving the heat transfer coefficient of the refrigerant in evaporation, condensation, and gas cooling [5,6]. This could be achieved actively or passively by means of twisted tapes, wire coils, ribs, fins, and dimples; surface vibration, fluid vibration, extended surfaces, coiled tubes, and treated surfaces [7]; and nanoparticles [8], which is this study's focus.

Nanoparticles are materials with one of the dimensions in nanoscale, and nanofluids are nanoparticle suspensions in a base fluid. Nanoparticles may be made from metals, metal oxides, a combination of both, or bio-based materials. Compared to their base fluids, nanofluids have relatively better heat transfer characteristics; however, this is associated with increased thermal conductivity. The increased aggregate viscosity of the nanofluid is the reason for the pressure drop increase. Conventional nanoparticles (Metallic, metal oxide) pose a threat to the environment as they rarely decompose, hence giving rise to the research of bio-nanoparticles. The commonly used bio-nanoparticle materials include banana, coconut, mango bark, mango leaf, palm kernel, etc.

A few experimental and numerical studies have looked into how nanoparticles and inclination angles affect the thermo-hydraulic performance of conventional base fluids. By changing the tube inclination angle, volume fraction, and Reynolds number of a constant heat flux flow from -90° to $+90^\circ$, 0.0%–2.0%, and 50 to 100, respectively, Uwadoka et al. [9] computationally examined the thermal and pressure drop properties of mango bark/CO_2 nanofluid. They found that the heat transfer coefficient increased with respect to volume fraction and Reynolds number and was maximum at the inclination angles of -30° and $+60^\circ$; however, the pressure drop increased as the volume fraction, and Reynolds number increased but exhibited minute sensitivity to inclination angle. Senthilkumar et al. [10] conducted an experiment to investigate the increase of the heat pipe's efficiency using copper nanofluid and de-ionized water as the working fluids while altering the heat input and pipe inclination angle. Efficiency peaked at the inclination angle of 45° for deionized water and copper nanofluid for all amounts of heat input under observation. The influence of tube inclinations and nanoparticle volume fraction on the thermodynamic parameters of the water-Al_2O_3 nanofluid was numerically investigated by Akbari

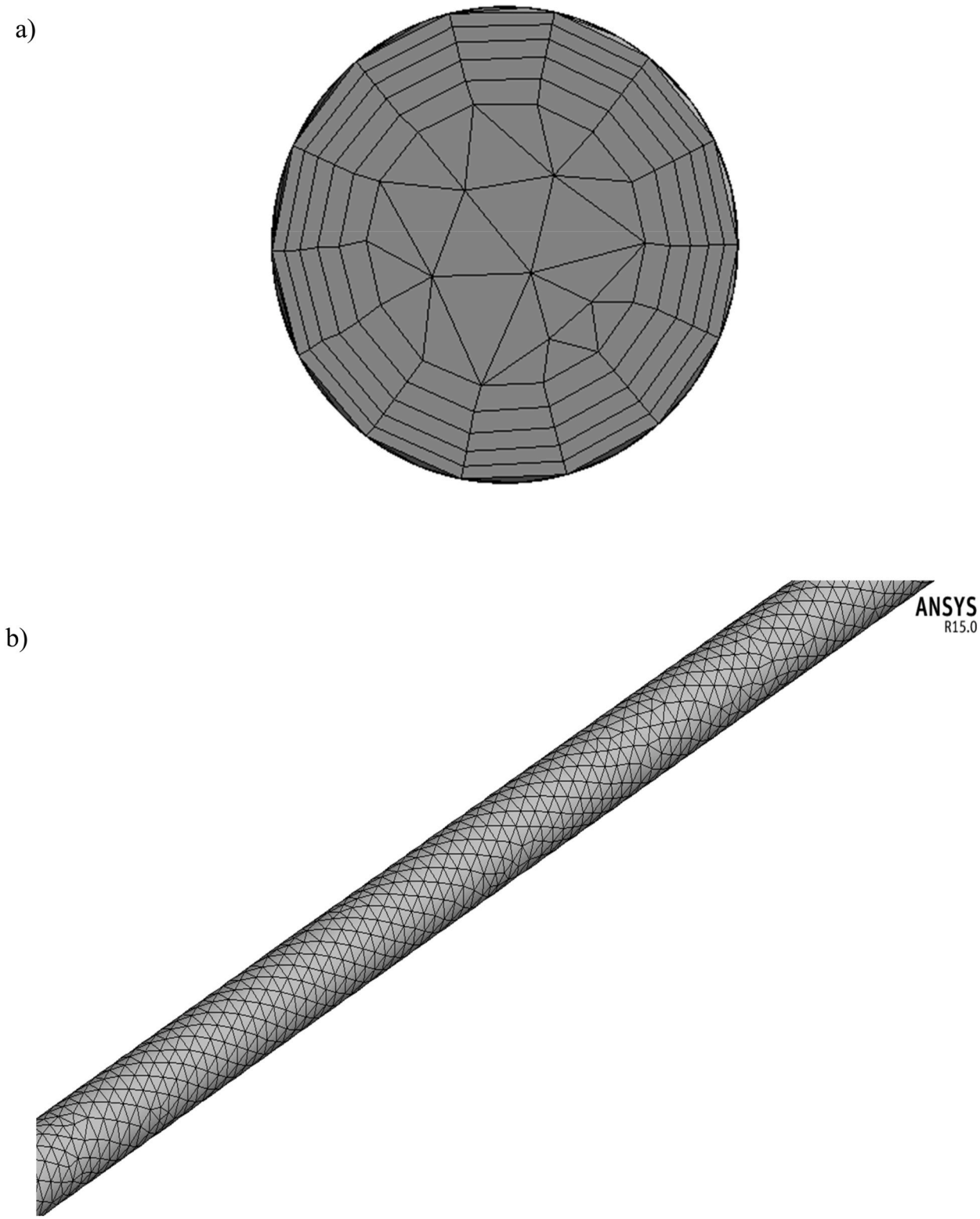

Fig. 2. Meshed models showing a) front view and b) isometric view.

Table 2
Grid independence test.

Mesh No. [−]	No. of meshes [−]	Exit wall temperature [K]	Comparison with previous grid [%]
i	19,499	314.61	
ii	38,597	321.9	2.32
iii	59,941	340.202	5.69
iv	101,166	335.057	1.51
v	234,971	329.626	1.62
vi	301,534	327.024	0.79%

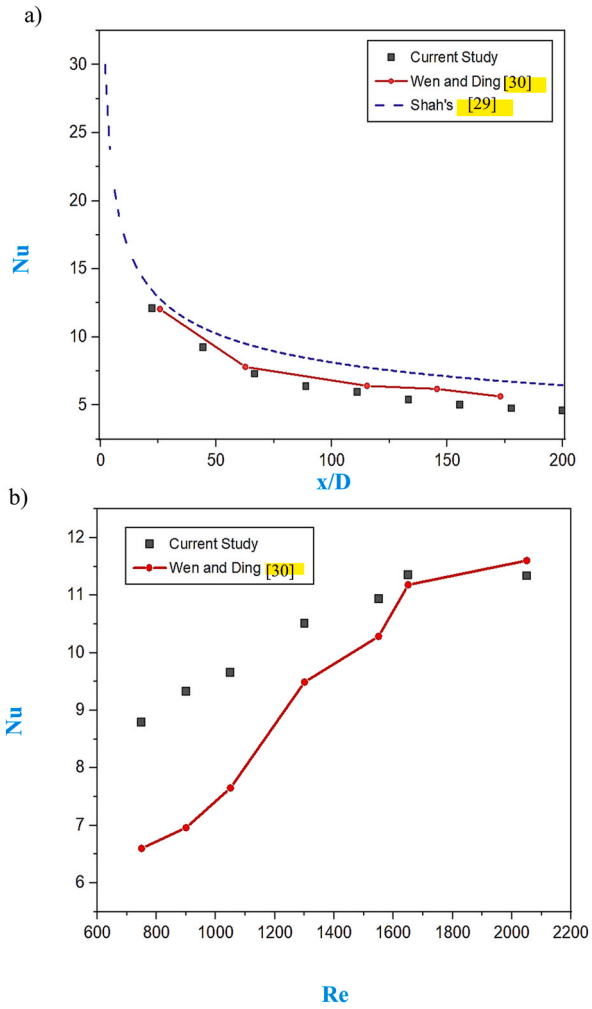

Fig. 3. Plots of (a) Nusselt number against axial distance (b) Nusselt number against Reynolds number, comparing this study, Shah's [29] equation, and Wen and Ding's [30] study.

et al. [11]. At a 4.0% volume fraction, the heat transfer coefficient increased by 15%, reaching a peak at 45° inclination angle. Karimipour et al. [12] investigated the laminar mixed convection of water-Cu nanofluid in an inclined shallow lid-driven cavity (LBM) using the lattice Boltzmann method. They discovered that at larger Reynolds number and volume fraction values, the maximum heat transfer rate could be achieved at the cavity's vertical position (inclination of 90°) at free convection domination (Richardson number = 10). Izadi et al. [13] investigated the effects of inclination angle and nanoparticle volume fraction on mixed convection of a lid-driven cavity, using Al_2O_3-water nanofluid as the working fluid. It was concluded that for Ricardson numbers of 1 and 100, the greatest cooling was achieved at an inclination angle of 315°. In order to examine the mixed convection of an Al_2O_3-water nanofluid inside a copper tube that had a uniform heat flux applied to its exterior, Mansour et al. [14] conducted an experimental study. The study's findings indicated that when the volume fraction increased from 0.0% to 4.0%, the heat transfer coefficient fell. Using a 1.0%

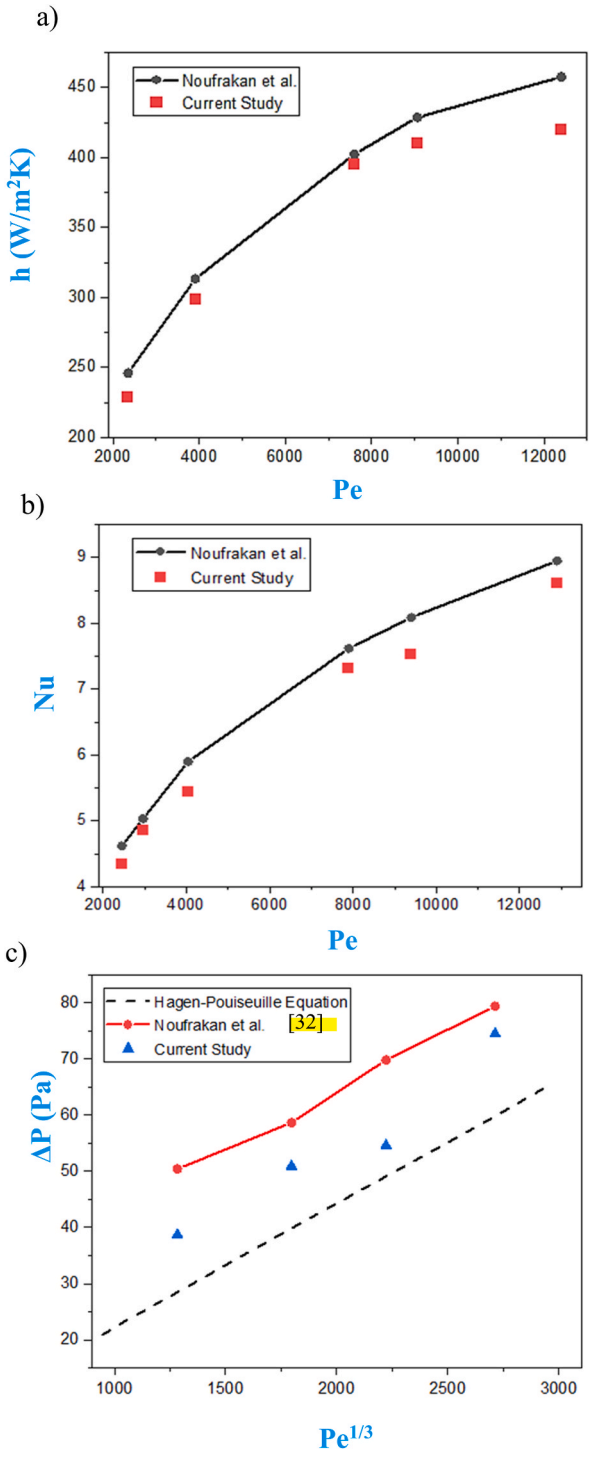

Fig. 4. Plots of (a) heat transfer coefficient against Peclet Number (b) Nusselt number against Peclet number, (c) pressure drop against cube root of Peclet number, comparing this study, Noufrakan et al. [32] study, and Hagen-Pouiselle Equation.

mass fraction of water/CuO, Liu et al. [15] conducted an experiment to examine how the inclination angle and operating pressure affected the thermal performance of a miniature inclined grooved heat pipe. According to experimental findings, the base fluid (water) and nanofluid exhibited optimal thermal performance at a temperature of 45 °C. Reji et al. [16] used deionized water and Al_2O_3-water nanofluid (with 1.0% volume fraction) as the working fluids to investigate a thermosyphon heat pipe in order to assess its thermal performance for various heat input values and angles of inclination. According to the study's findings, using the nanofluid instead of DI

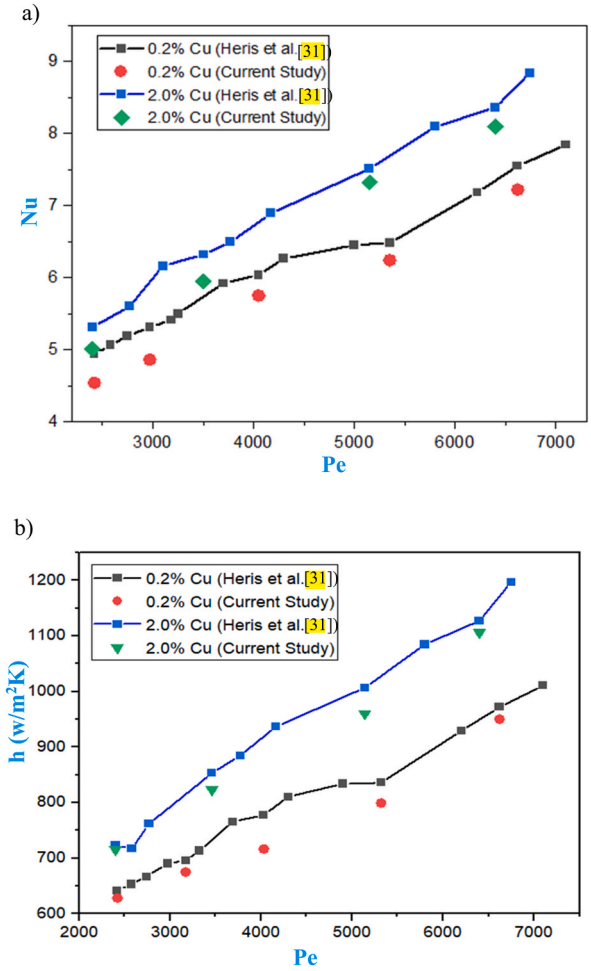

Fig. 5. Plots of (a) Nusselt number against Peclet number (b) heat transfer coefficient against Peclet number, comparing this study and Heris et al. [31] study.

Table 3
Error Measurements between this study and the validated studies.

Study validated	Working fluid/ nanofluid	parameter [−]	MSE [%]	RMSE [%]	MAD [%]
Shah [29]	Water	Nu vs. x/D	2.745	1.657	31.450
Wen and Ding [30]	Water	Nu vs. Re	3.412	1.847	13.990
Heris et al. [31]	0.2% vol. Cu/water	Nu vs. Pe	0.122	0.350	6.306
	2.0% vol. Cu/water	Nu vs. Pe	0.084	0.290	5.181
	0.2% vol. Cu/water	h vs. Pe	1440.526	37.954	4.110
	2.0% vol. Cu/water	h vs. Pe	896.567	29.943	2.885
Noufrakan et al. [32]	0.2% vol. CuO/water	h vs. Pe	447.542	21.160	5.352
	0.2% vol. CuO/water	Nu vs. Pe	0.139	0.373	5.614
	2.0% vol. CuO/water	ΔP vs. Peˆ1/3	112.883	10.620	19.953

water resulted in a 41.0% improvement in the heat pipe's performance, and a peak efficiency of 88.0% was seen at a 60° inclination angle. Aly et al. [17] conducted an experiment employing distilled water and alumina/water nanofluid with a vol. proportion of 3.0% to determine the effects of tube inclination angle, filling ratio, and heat input on the heat transfer capabilities of a helically-micro-grooved heat pipe. They discovered that, either using water or a nanofluid, inclining the heat pipe at an angle of 60° produced the optimum thermal results. Bartelt et al. [18] examined the flow boiling of CuO nanoparticles distributed in a mixture of R134a/polyol/easter oil. They noted that a nanofluid with a 0.5% weight concentration had little impact on improving heat transfer, but one with a 1.0% mass fraction increased heat transfer by 42–82%.

Furthermore, a 2.0% mass fraction showed an increase in heat transfer of 50–101%. Henderson et al. [19] investigated the effect of

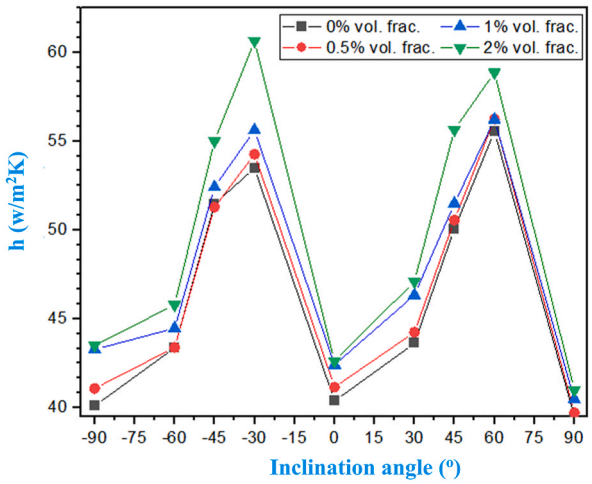

Fig. 6. Heat transfer coefficient versus inclination angle for Re = 100.

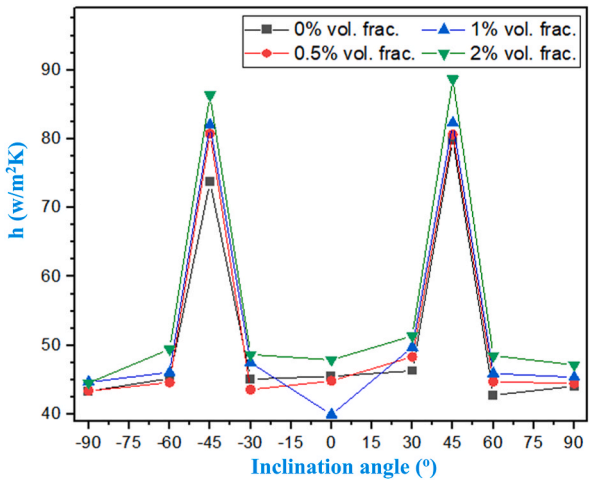

Fig. 7. Heat transfer coefficient versus inclination angle for Re = 400.

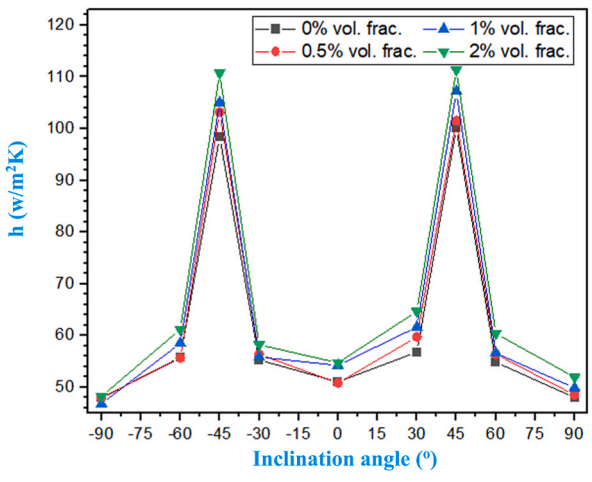

Fig. 8. Heat transfer coefficient versus inclination angle for Re = 700.

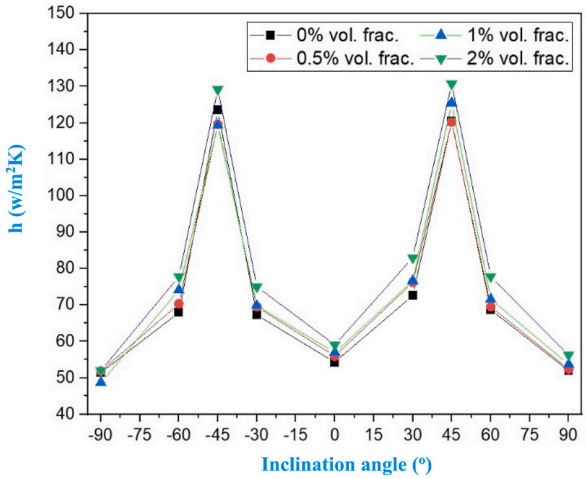

Fig. 9. Heat transfer coefficient versus inclination angle for Re = 1000.

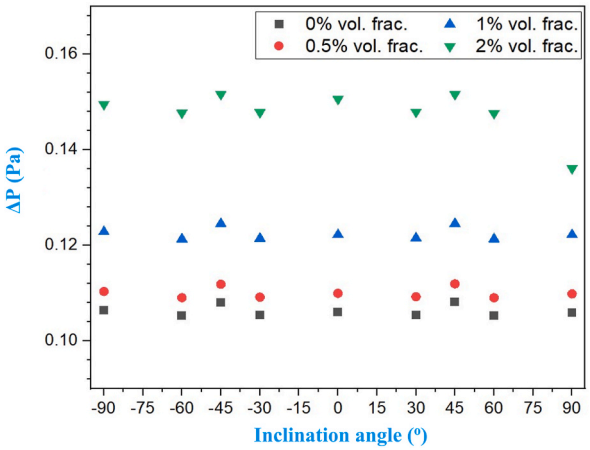

Fig. 10. Pressure drop versus inclination angle for Re = 100.

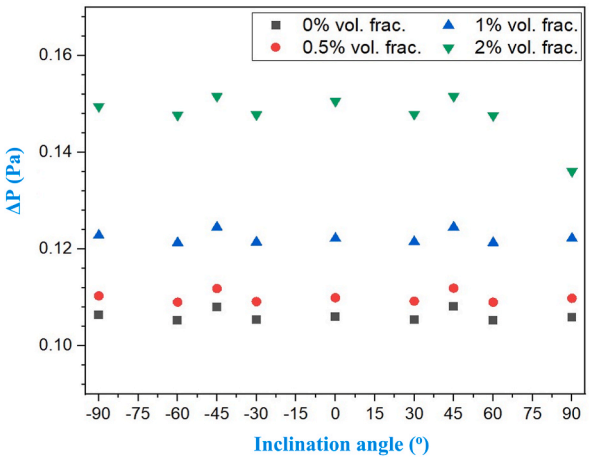

Fig. 11. Pressure drop versus inclination angle for Re = 400.

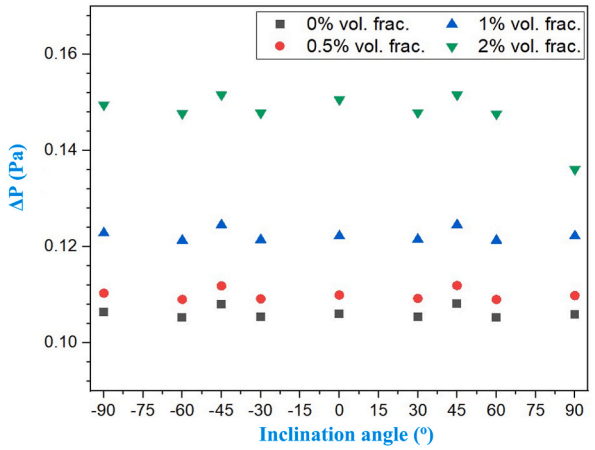

Fig. 12. Pressure drop versus inclination angle for Re = 700.

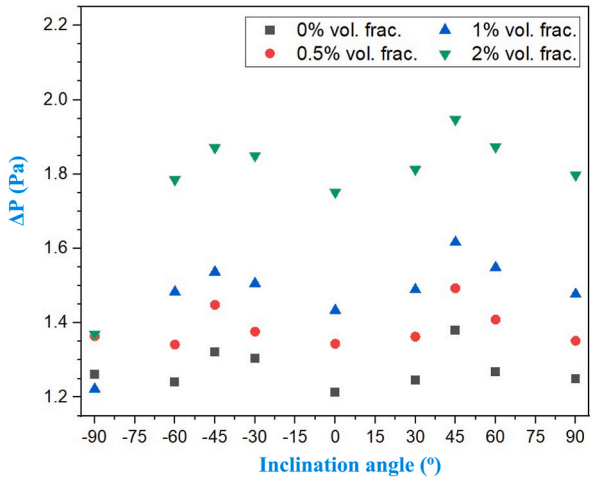

Fig. 13. Pressure drop versus inclination angle for Re = 1000.

SiO_2 nanoparticles on the boiling heat transfer coefficient of R-134a and R-134a/polyolester in a two-phase flow with a volume fraction of 0.02%–0.08%. In comparison to pure R-134a refrigerant, the heat transfer coefficient was reduced by 55% when nanoparticles were combined with it through direct dispersion.

On the subject of entropy production of nanofluids in refrigeration, Mah et al. [20] conducted an analytical investigation on the impact of viscous dissipation on entropy formation in water-alumina nanofluid forced convection in circular microchannels. In this study, mathematical models premised on the first and second laws of thermodynamics were developed. In both laminar and turbulent regimes, Moghaddami et al. [21] investigated the impact of increasing nanoparticles on the formation of entropy in a water/Al_2O_3 nanofluid flowing through a circular pipe with a uniform wall heat flux boundary condition. In the laminar regime, it was found that a volume fraction of 1.0% for water-Al_2O_3 reduced entropy production by 3.6%, and the maximum entropy production reduction was approximately 18.0% for a volume fraction of 5.0% and Reynolds number of 853. Li and Kleinstreuer [22] used a computer-simulated model to examine the entropy production rates in laminar microchannel flow for the steady flow of pure water and CuO/water nanofluids. The results showed that system entropy production decreased as fluid inlet temperature increased, reducing local temperature gradients. The heat transfer-induced entropy production predominated under high heat flux conditions. Furthermore, nanofluids with extremely low volume fractions of metal nanoparticles were excellent coolants and further reduced system entropy production rates at lower Reynolds numbers due to their superior thermal properties. Ebrahimi et al. [23] evaluated conjugate heat transfer and flow performance for nanofluid in a rectangular-shaped microchannel heat sink with longitudinal vortex generators at various Reynolds numbers. It was discovered that for Al_2O_3/water and CuO/water nanofluids, respectively, total efficiency was increased by 2.55%–29.05% and 9.78%–50.64%. Heshmatian and Bahiraei [24] investigated the irreversibilities brought on by heat transport and fluid friction that cause entropy to be generated in water-TiO_2 nanofluid. They noted that when the particle size and mean concentration increased, the particle migration also increased.

Additionally, because friction, a primary factor in entropy formation in the microchannel, drops with increasing particle size, the

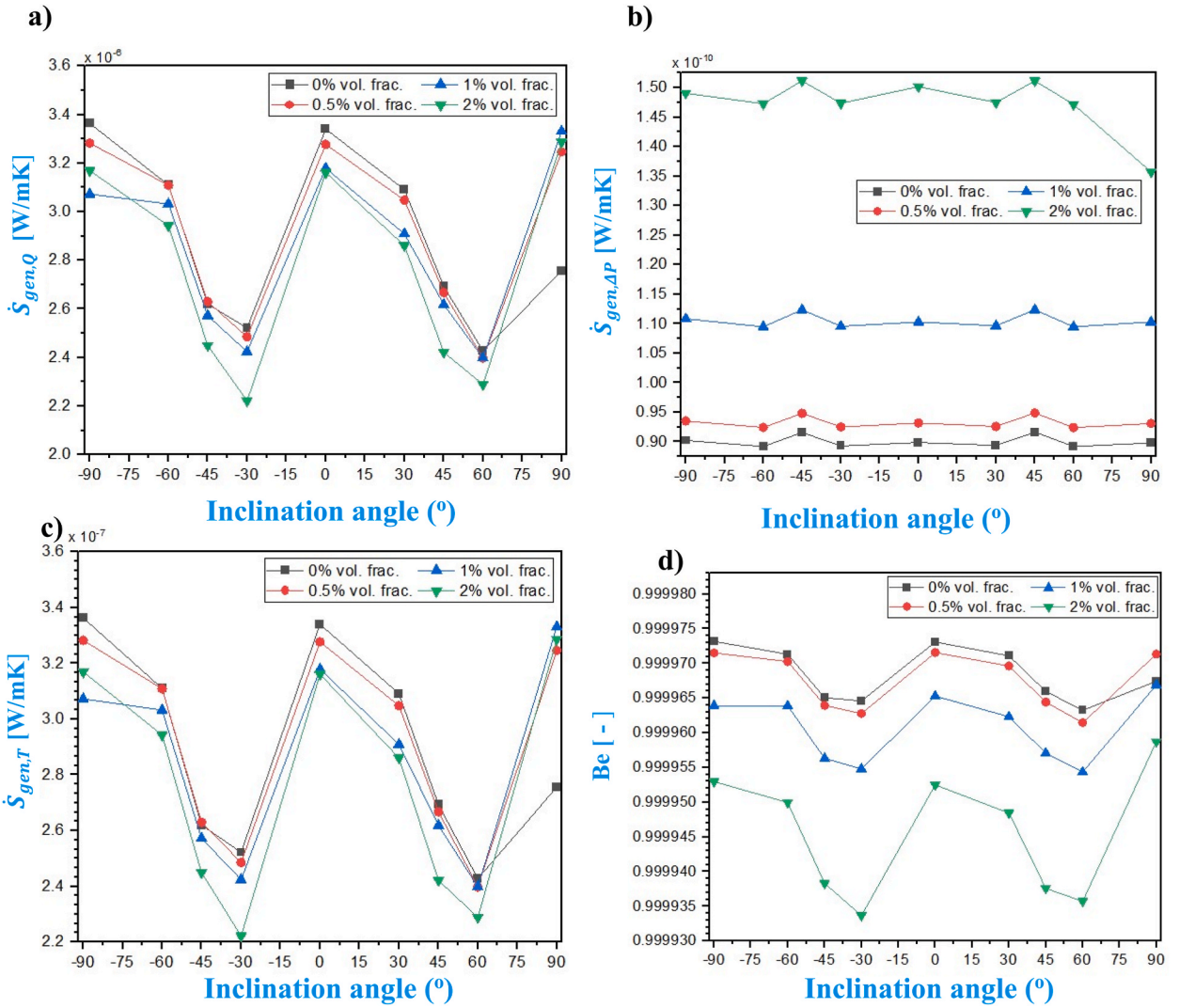

Fig. 14. Entropy production rates versus tube inclination angle for a) heat transfer, b) pressure drop, c) total, and d) Bejan number for various nanofluid volume fractions for Re = 100.

total entropy production rate also decreases. Among other things, Yang et al. [25] investigated how the volume fraction and Reynolds number influenced the production of entropy of nanofluids in a trapezoidal microchannel. The results showed that while the system's dimensionless thermal entropy production rate decreased with increasing Reynolds number, it increased with increasing friction entropy production rate. Using two operating fluids in the hot and cold channels (water and Al_2O_3/water nanofluid), Mohammadian et al. [26] numerically investigated the entropy production in a counterflow microchannel heat exchanger (CFMCHE). The findings demonstrated that the profiles for the frictional contribution of entropy production were opposite those for the heat transfer contribution of entropy production and that they increased with reduced particle size and increased volume fraction. Total entropy production declined as particle size and volume fraction increased, with the best performance occurring at smaller particle sizes and greater volume fractions. Sohel et al. [27] carried out an analytical study on the production of entropy in a turbulent flow employing two different base fluids (ethylene glycol and water) and two different types of nanoparticles (Cu and Al_2O_3). They came to the conclusion that as the volume fraction increased, entropy production decreased. They also found that the entropy production rate ratio in the microchannel was less than unity and reduced by the increasing volume fraction. In contrast, the entropy production rate ratio in the minichannel was greater than the unity for Al_2O_3/water and Al_2O_3/EG nanofluids.

For a better understanding of the effect of gravitational forces on the performance of heat exchange systems for a sustainable urban environment, more research is needed on the heat transfer coefficient, pressure drop and entropy production rates of bionanofluids in inclined flow be it laminar or turbulent. To the best of the authors' knowledge, studies on the influence of inclination angle (i.e. gravitational force) on CO_2-based mango bark nanofluid flow inside in-tube heat exchanger is rare in the literature [9]. This paper, therefore, seeks to fill the gap by investigating the effect of inclination angle, Reynolds number, and volume fraction on the heat

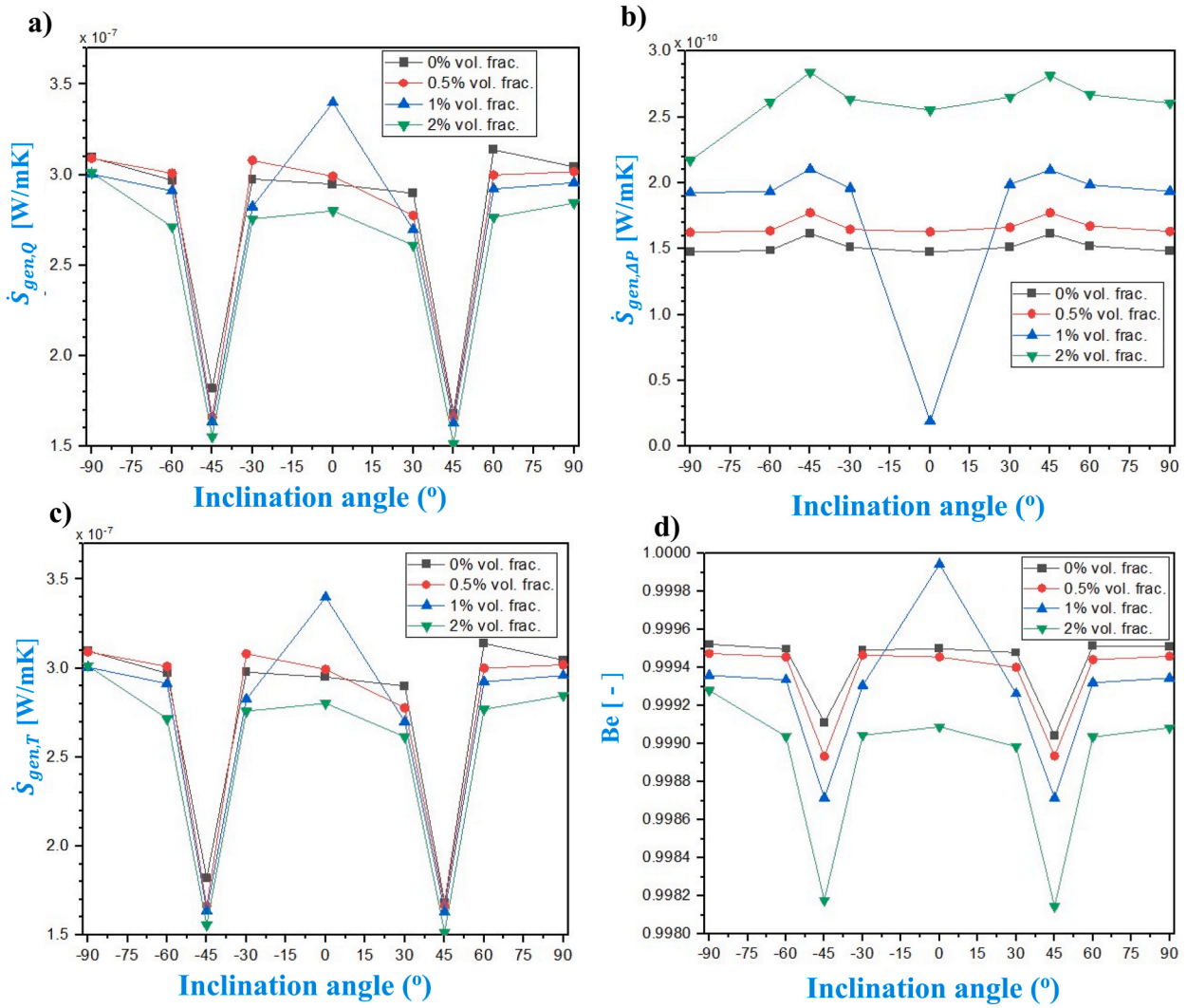

Fig. 15. Entropy production rates versus tube inclination angle for a) heat transfer, b) pressure drop, c) total, and d) Bejan number for various nanofluid volume fractions for Re = 400.

transfer, pressure drop, and entropy production properties of mango bark/CO_2 nanofluid in a laminar flow regime. This study uses ANSYS Fluent as a computational fluid dynamics (CFD) simulation tool to carry out the investigation.

2. Description of simulation parameters

This study focuses on the flow of mango bark/CO_2 nanofluid at 320.0 K through a tube with an inner radius of 2.25 mm and length of 970.0 mm. The tube is given a heat flux of -10.0 W/m^2 at its walls. The interest of the study is in the laminar flow regime with Reynolds numbers of 100, 400, 700, and 1000. The direction and inclination of flow are also considered for the following angles; $\pm 90°$, $\pm 60°$, $\pm 45°$, $\pm 30°$, $0°$. Lastly, the volume fractions used are 0.5%, 1.0%, and 2.0%. Fig. 1 shows a schematic diagram of the simulated model.

3. Mathematical models

The bionanofluid is in a single phase, and the problem presented deals with flow and heat transfer, hence, the continuity, momentum, and energy equations apply as given in Eqs. (1)–(5).

$$\frac{\partial}{\partial r}(ru_r) + \frac{\partial}{\partial \theta}(u_\theta) + r\frac{\partial}{\partial z}(u_z) = S_m \Big/ \rho \tag{1}$$

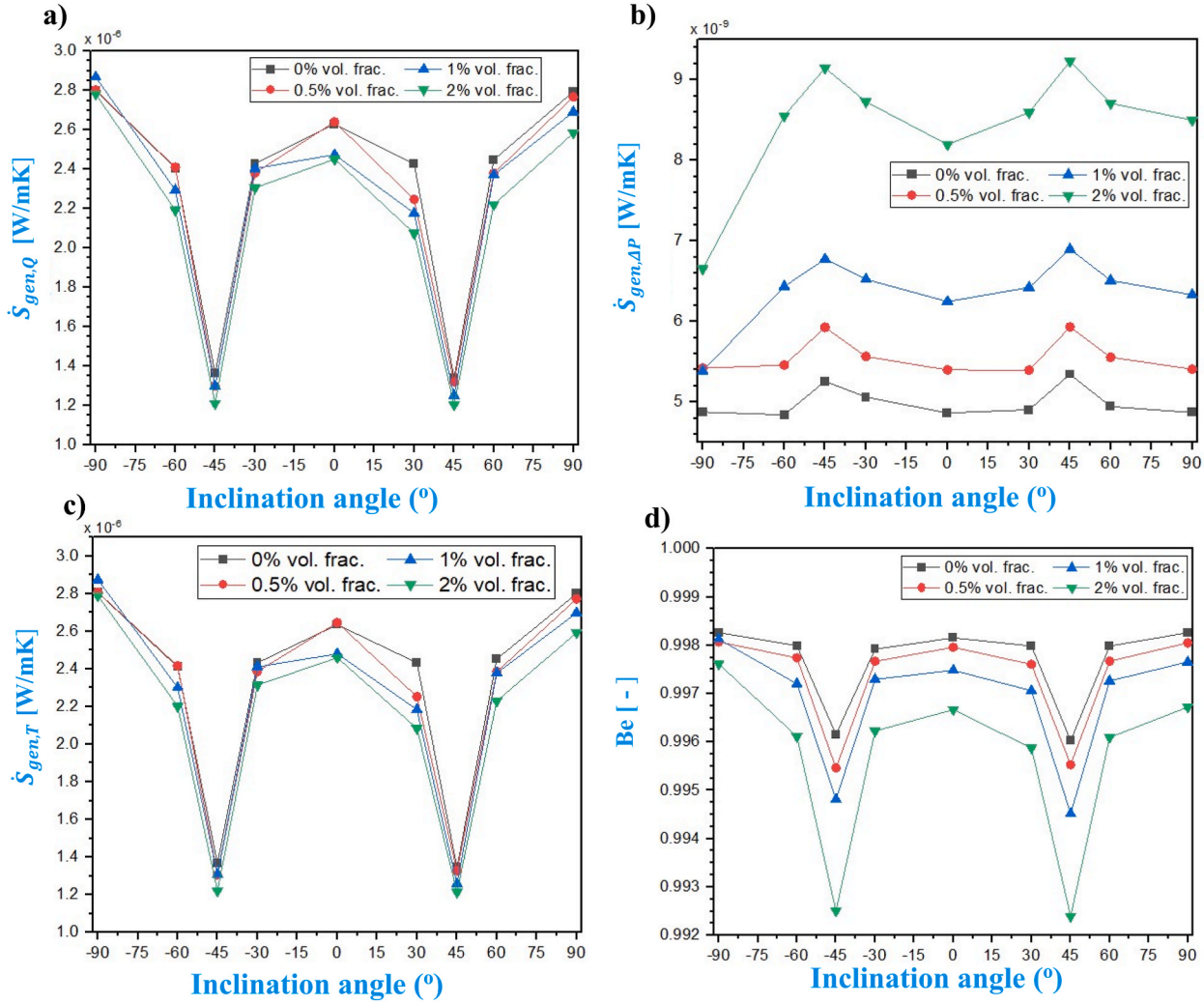

Fig. 16. Entropy production rates versus tube inclination angle for a) heat transfer, b) pressure drop, c) total, and d) Bejan number for various nanofluid volume fractions for Re = 700.

$$\rho\left(\frac{\partial u_r}{\partial t}+u_r\frac{\partial u_r}{\partial r}+\frac{u_\theta}{r}\frac{\partial u_r}{\partial \theta}+u_z\frac{\partial u_r}{\partial z}-\frac{u_\theta^2}{r}\right)=-\frac{\partial p}{\partial r}+\mu\left[\frac{\partial}{\partial r}\left(\frac{1}{r}\frac{\partial}{\partial r}(ru_r)\right)+\frac{1}{r^2}\frac{\partial^2 u_r}{\partial \theta^2}+\frac{\partial^2 u_r}{\partial z^2}-\frac{2}{r^2}\frac{\partial u_\theta}{\partial \theta}\right]+\rho g_r+F_r \tag{2}$$

$$\rho\left(\frac{\partial u_\theta}{\partial t}+u_r\frac{\partial u_\theta}{\partial r}+\frac{u_\theta}{r}\frac{\partial u_\theta}{\partial \theta}+u_z\frac{\partial u_\theta}{\partial z}+\frac{u_r u_\theta}{r}\right)=-\frac{1}{r}\frac{\partial p}{\partial \theta}+\mu\left[\frac{\partial}{\partial r}\left(\frac{1}{r}\frac{\partial}{\partial r}(ru_\theta)\right)+\frac{1}{r^2}\frac{\partial^2 u_\theta}{\partial \theta^2}+\frac{\partial^2 u_\theta}{\partial z^2}+\frac{2}{r^2}\frac{\partial u_r}{\partial \theta}\right]+\rho g_\theta+F_\theta \tag{3}$$

$$\rho\left(\frac{\partial u_z}{\partial t}+u_r\frac{\partial u_z}{\partial r}+\frac{u_\theta}{r}\frac{\partial u_z}{\partial \theta}+u_z\frac{\partial u_z}{\partial z}\right)=-\frac{\partial p}{\partial z}+\mu\left[\frac{1}{r}\frac{\partial}{\partial r}\left(r\frac{\partial u_z}{\partial r}\right)+\frac{1}{r^2}\frac{\partial^2 u_z}{\partial \theta^2}+\frac{\partial^2 u_z}{\partial z^2}\right]+\rho g_z+F_z \tag{4}$$

$$\frac{\partial}{\partial t}(\rho E)+\nabla\cdot(\vec{u}(\rho E))=\nabla\cdot(k\nabla T)+S_h \tag{5}$$

3.1. Thermophysical properties of the bionanofluid

The physical properties of the bionanofluid studied at various volume fractions are computed using the following relations (Eqs. (6)–(9)) for each property obtained from the study done by Kakaç and Pramuanjaroenkij [28]. The computed thermophysical properties are given in Table 1.

$$\rho_{nf}=\varphi\,\rho_p+(1-\varphi)\rho_f \tag{6}$$

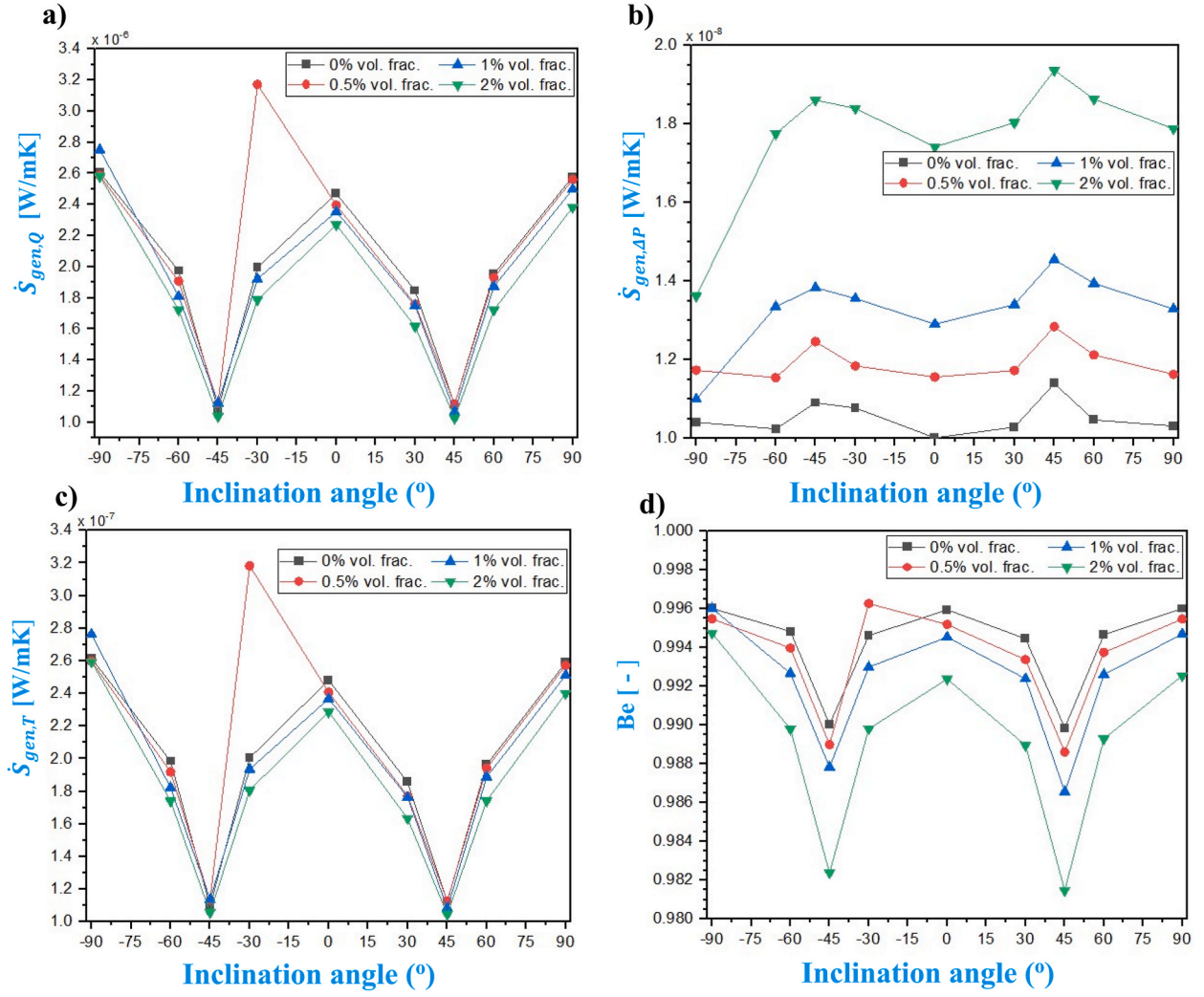

Fig. 17. Entropy production rates versus tube inclination angle for a) heat transfer, b) pressure drop, c) total, and d) Bejan number for various nanofluid volume fractions for Re = 1000.

$$\mu_{nf} = \mu_f(1 + 2.8\varphi) \tag{7}$$

$$C_{p\,nf} = \frac{\varphi\,\rho_p C_{p\,p} + (1-\varphi)\rho_f C_{p\,f}}{\rho_{nf}} \tag{8}$$

$$k_{nf} = k_f\left(\frac{k_p + 2\,k_f + 2\,\varphi\,(k_f - k_p)}{k_p + 2\,k_f - 2\,\varphi\,(k_f - k_p)}\right) \tag{9}$$

3.2. Boundary conditions and setup

At the inlet, the fluid temperature is set to 320.0 K, and velocity is determined by the Reynolds number Re using Eq. (10). A constant heat flux of -10.0 W/m^2 is applied on the wall of the tube, and the outlet is set to outflow in ANSYS-Fluent environment. The solution method is set to SIMPLE, and all residuals are set to 1×10^{-6}. The discretized model fed to the simulation software is shown in Fig. 2. Re is related to the velocity and other properties of the fluid, as presented in Eq. (10)

$$\mathrm{U} = \frac{\mathrm{Re}\,\mu_{\mathrm{nf}}}{\mathrm{D}\rho_{\mathrm{nf}}} \tag{10}$$

where ρ_{nf}, μ_{nf}, and D are the bionanofluid density, viscosity, and tube inner diameter, respectively.

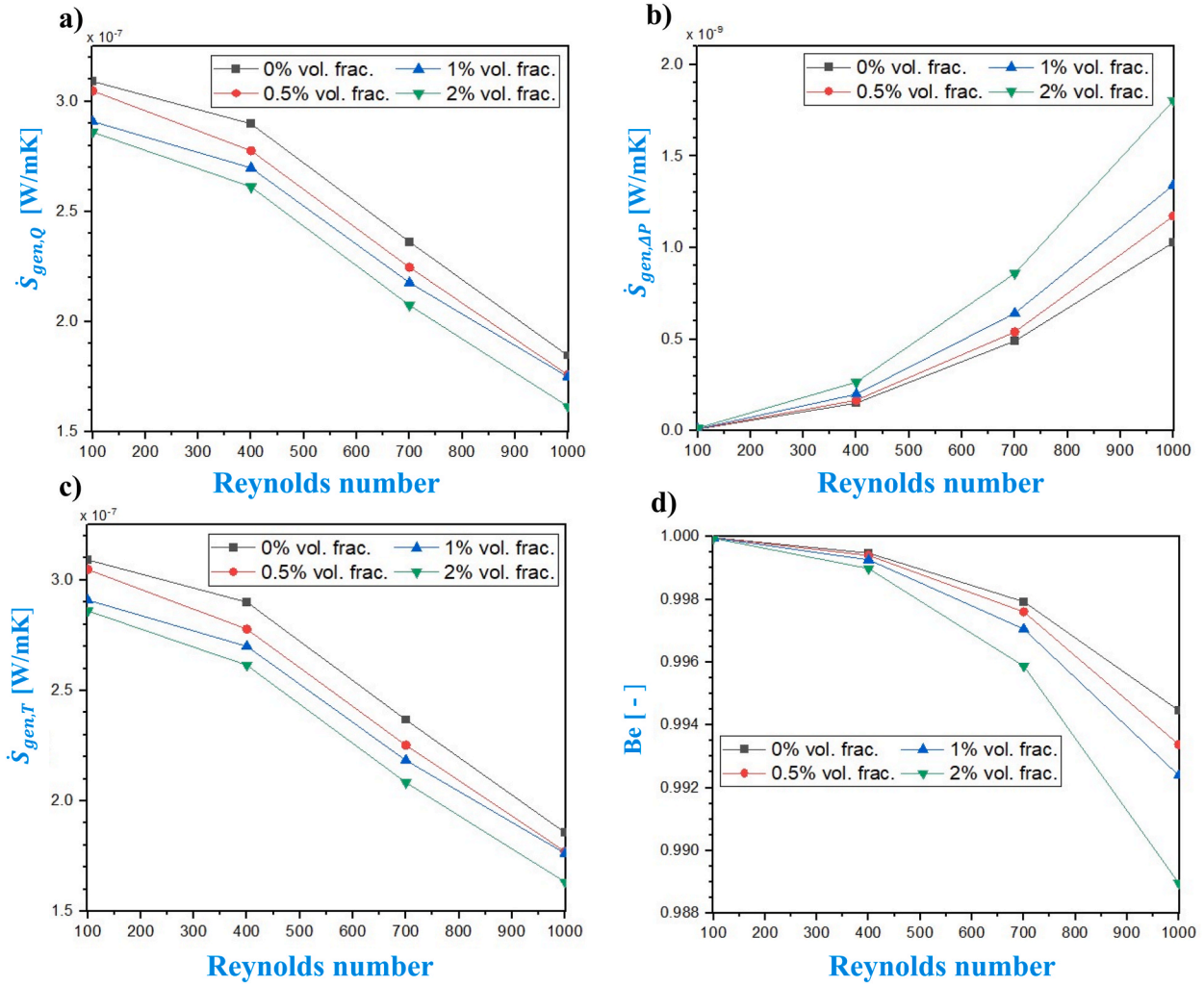

Fig. 18. Entropy production rates versus Reynolds number for a) heat transfer, b) pressure drop, c) total, and d) Bejan number for various nanofluid volume fractions for $\beta = +30.^{o}$

3.3. Data processing

Since this study relies on CFD simulation, raw data from the simulated scenarios are used to generate particulars on the fluid's heat transfer coefficient, pressure difference, and entropy production rates. The pressure drop is calculated by finding the difference between the inlet and outlet pressures as demonstrated in Eq. (11), and the heat transfer coefficient h is calculated using Eq. (12)

$$\Delta P = P_{in} - P_{out} \tag{11}$$

$$h = \frac{q}{T_w - T_b} \tag{12}$$

where q is the heat flux, T_w the wall temperature, and T_b the fluid bulk temperature.

Entropy production rates, with regards to heat transfer, frictional pressure drop, the addition of the two, and Bejan number, can be calculated using Eqs. (13)–(16).

The heat transfer contribution to entropy production is given as:

$$\dot{S}_{gen,Q} = \frac{\dot{Q}\Delta T}{T_b^2} \tag{13}$$

where $\dot{Q} = \text{Iv}\pi\text{DL}$ and ΔT is temperature difference. The frictional pressure contribution to the entropy production rate is expressed as:

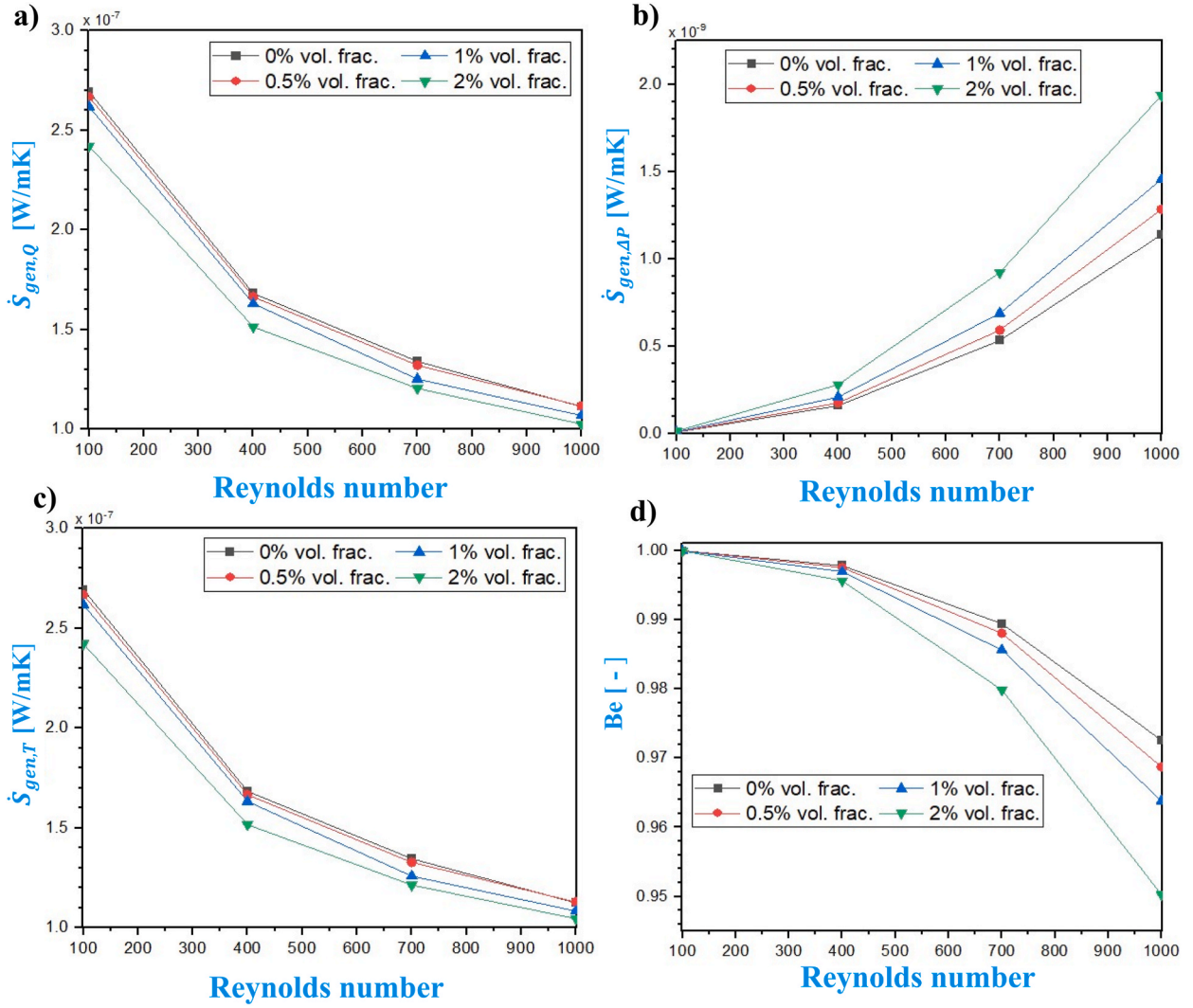

Fig. 19. Entropy production rates versus Reynolds number for a) heat transfer, b) pressure drop, c) total, and d) Bejan number for various nanofluid volume fractions for $\beta = +45.^{o}$

$$\dot{S}_{gen,\Delta P} = \frac{\dot{m}\Delta P_{fric}}{\rho_{nf}\, T_b} \tag{14}$$

where ṁ is the mass flow rate. The total entropy production is:

$$\dot{S}_{gen,T} = \dot{S}_{gen,Q} + \dot{S}_{gen,\Delta P} \tag{15}$$

The Bejan number is obtained by dividing the heat transfer entropy produced by the total entropy produced and it is expressed as:

$$Be = \frac{\dot{S}_{gen,Q}}{\dot{S}_{gen,T}} \tag{16}$$

3.4. Grid independence study

A grid analysis was done for a number of finite-volume meshes with various numbers of elements, with the deviation - $\left|\frac{\Delta h_i - \Delta h_{i-1}}{\Delta h_i}\right| \leq$ 1%. Table 2 displays the outcomes of the grid independence test. It can be observed from the data in the table that the difference between mesh numbers 5 and 6 is 0.79%. Due to this, the mesh smoothness of all simulations conducted for this study is the same as Mesh v. Furthermore, it was noted that increasing the number of meshes after mesh number vi results in divergence.

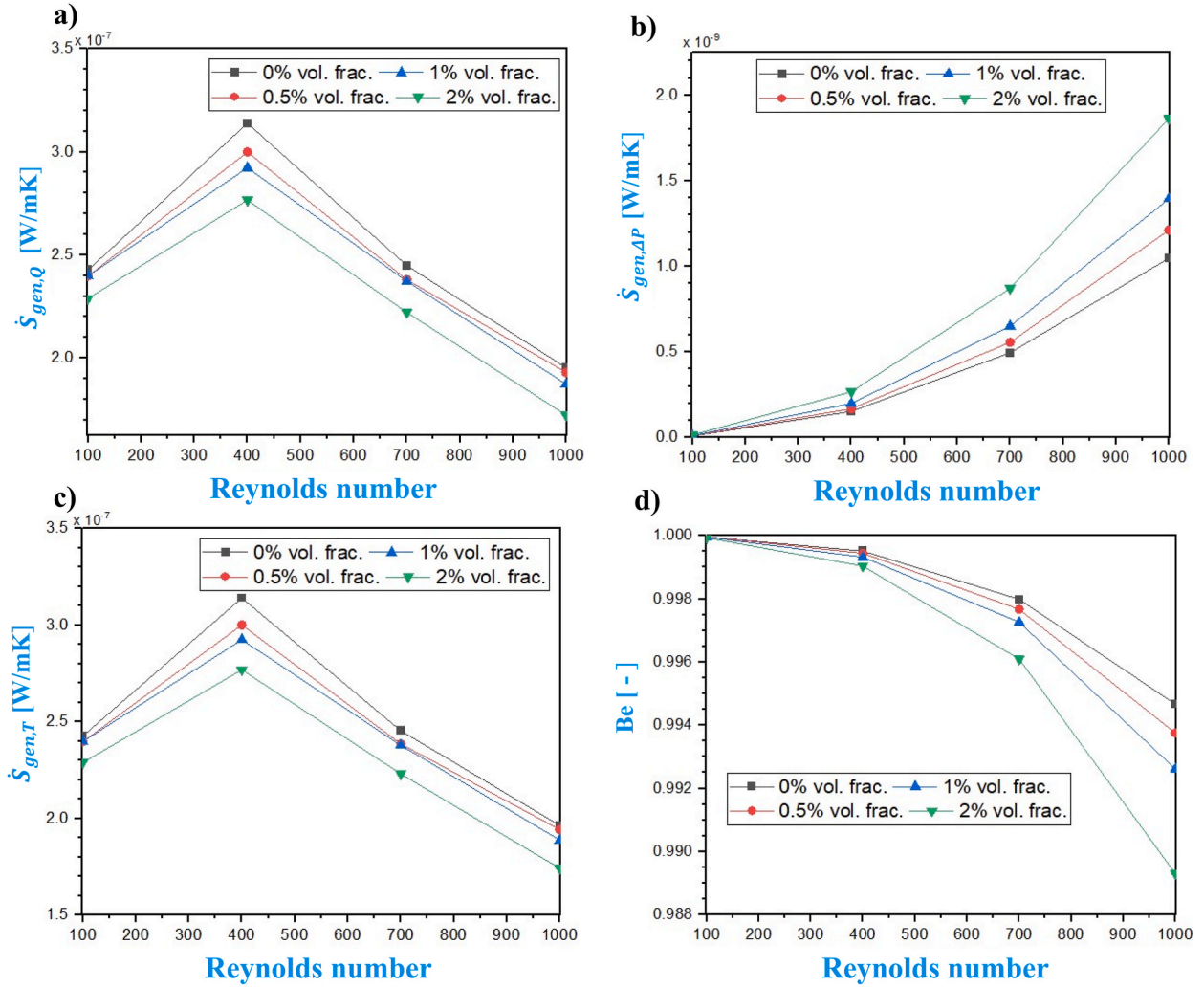

Fig. 20. Entropy production rates versus Reynolds number for a) heat transfer, b) pressure drop, c) total, and d) Bejan number for various nanofluid volume fractions for $\beta = +60.^{o}$

4. Code validation

The dependability of the simulation setup was ensured before starting a systematic investigation on the bionanofluid of interest. For ease of comparison, statistical analysis was done using the mean absolute deviation (MAD), mean square error (MSE), and root mean square error (RMSE). The results were also compared to the Shah [29] equation for laminar flows with a constant heat flux boundary condition shown in Eq. (17); experimental results of the investigation done on the heat transfer coefficient of water under laminar conditions [30], heat transfer coefficient of Cu/Water nanofluids through a circular tube [31], and experimental study of heat transfer coefficient and pressure drop of CuO/water nanofluid [32].

$$Nu = \begin{cases} 1.935\left(Re.Pr\,\frac{x}{D}\right)^{1/3}\left(Re.Pr\,\frac{D}{x}\right) \geq 33.3 \\ 4.364 + 0.0722\,Re.Pr\,\frac{D}{x} \quad \left(Re.Pr\,\frac{D}{x}\right) < 33.3 \end{cases} \tag{17}$$

The plots in Fig. 3, Fig. 4 and Fig. 5 show a strong correlation between this current study and the validated studies. Table 3 provides these correlations in the form of error measurements. From Table 3, the largest mean absolute deviation is with Shah [29] equation at 31.45%. Although the exact reason for this is unknown, this significant error could be due to the Shah [29] equation designed for tubes of bigger radii. The MAD for all other studies is within ±20%.

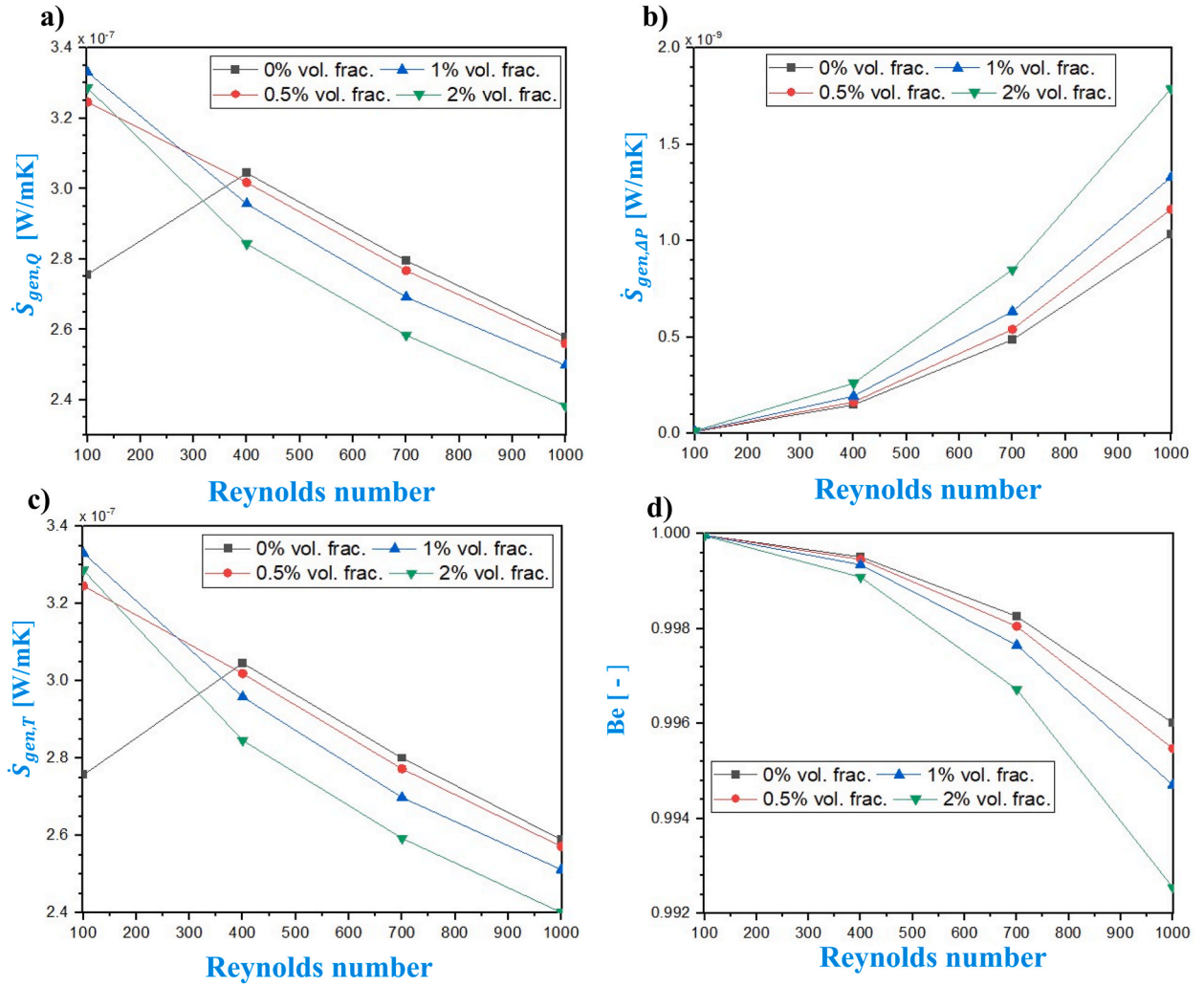

Fig. 21. Entropy production rates versus Reynolds number for a) heat transfer, b) pressure drop, c) total, and d) Bejan number for various nanofluid volume fractions for $\beta = +90.^{o}$

5. Results and discussion

This section discusses how the tube inclination angle, volume fraction, and Reynolds number affect the mango bark/CO_2 nanofluid's heat transfer, pressure drop properties, and entropy production rates. The Reynolds number is changed from 100 to 1000; the volume fraction of nanoparticles in the sample from 0.0% to 2.0%; and the inclination angle from -90° to $+90^{\circ}$. Positive angles denote upward flow (against gravity), and negative angles indicate downward flow (in the direction of gravity). An inclination angle of 0° represents horizontal tube orientation. The overview of the result shows that the inclination angle significantly impacts the rate of entropy formation and heat transfer coefficient, while the pressure drop is barely affected. The minute effect of the inclination angle on the pressure drop could be due to the comparatively small change in the static pressure with the inclination angle.

5.1. Thermal performance: effects of tube inclination angle and volume fraction

Figs. 6–9 provide charts illustrating the variation in the heat transfer coefficient with respect to the inclination angle for different volume fractions and Reynolds numbers. It is clear that for all Reynolds numbers, the heat transfer coefficients and inclination angle have a similar relationship. The results further show that the thermal performance significantly rises with the nanofluid volume fraction, primarily due to increased particle intercollision forces brought about by the Brownian motion and inertia force. Other studies reported the increase in the thermal performance of different nanofluids, for instance, Onyiruika et al. [33,34] mango bark-water, and Omosehin et al. [35,36] alumina and Cu hybrid in water suspension. As expected, the greatest heat transfer coefficient is often given at a volume fraction of 2.0%. Furthermore, at a high volume fraction, the thermal boundary layer is reduced, the axial conduction increased, and thermal resistance decreased. The heat transfer coefficient rises with inclination angle starting from -90° for all

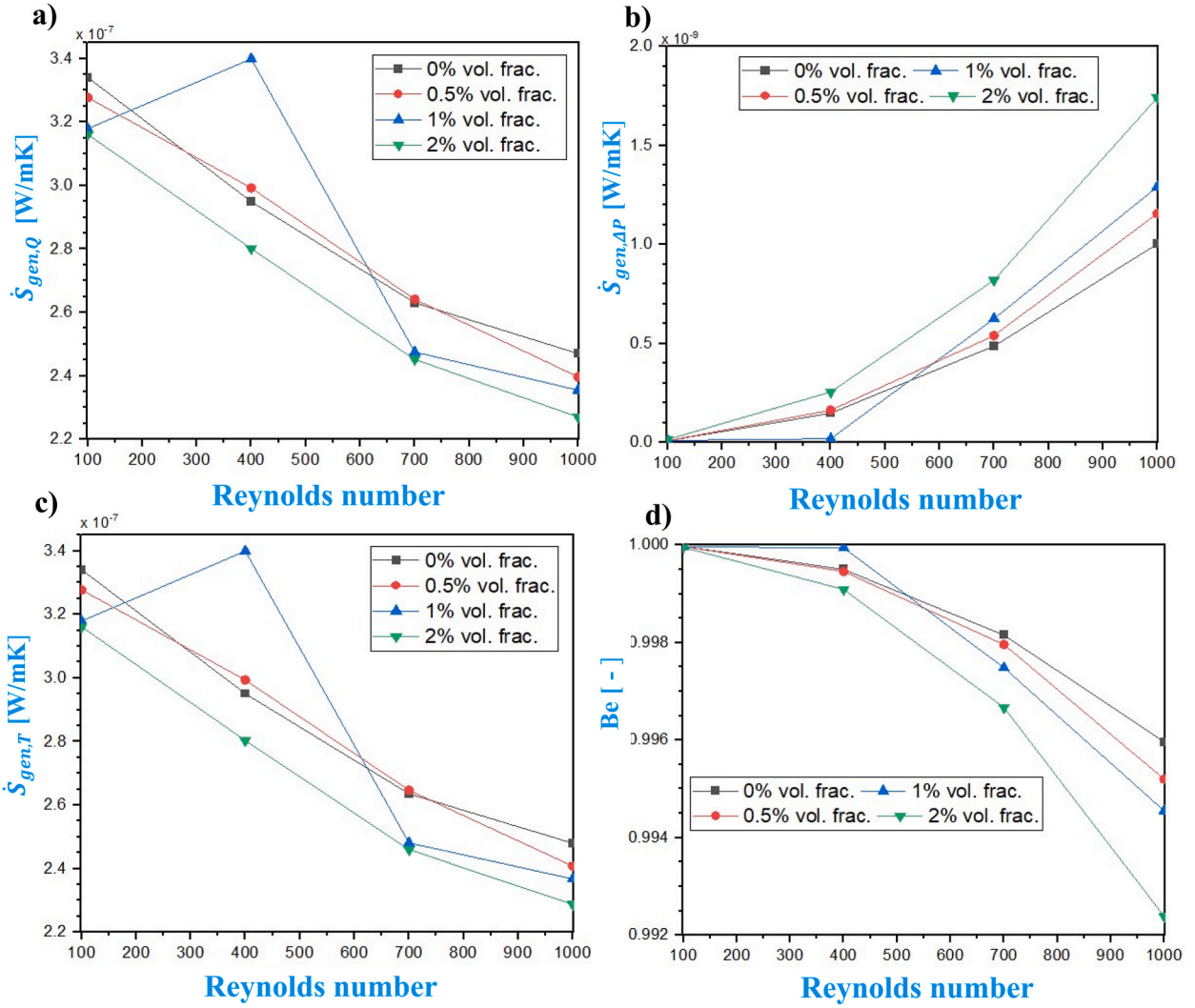

Fig. 22. Entropy production rates versus Reynolds number for a) heat transfer, b) pressure drop, c) total, and d) Bejan number for various nanofluid volume fractions for $\beta = 0.^{o}$

Reynolds numbers. For Reynolds number greater than 100, it reaches its highest point at the angle of $-45°$, dips to a low at $0°$, rises once more to peak at $+45°$, and then drops to another low at $+90°$ (Figs. 7–9). The oscillatory tendency remains true for Reynolds numbers of 100, but the peaks are rather at the angles of $-30°$ and $+60°$ (Fig. 6). The heat transfer coefficient's lowest values typically occur at the inclination angles of 0o and $\pm 90°$. As the inclination angle changes between $-90°$ and $-45°$ and $0°$ and $+45°$ and peaks at $\pm 45°$, the increase in the heat transfer coefficient could be due to the reduced thermal boundary layer by the gravitational force [37]. Beyond the peak, the impact of the gravitational force on the thermal boundary layer degrades and the temperature difference between the surface and bulk fluid increases thereby increasing the thermal resistance [37,38]. Uwadoka et al. [9], Senthilkumar et al. [10], and Akbari et al. [11] also reported a peak value at an inclination angle of $+45°$, while Uwadoka et al. [9] also noted a peak at the inclination angle of $-30°$, $-45°$, and $+60°$ depending on the Reynolds number. The percentage thermal enhancements are 42%, 93.98%, 121.28%, and 150% for Reynolds numbers of 100, 400, 700, and 1000, respectively.

5.2. *Pressure drop: effects of tube inclination angle and volume fraction*

Plots of the pressure drop change with respect to tube inclination angle for different volume fractions and Reynolds numbers are shown in Figs. 10–13. The results show a distinct relationship between the pressure drop and volume fraction of the bionanofluid. In all cases, the pressure drop increases as the volume fraction increases, with the maximum pressure drop corresponding to 2.0% and the minimum to 0.0% volume fraction. The increased viscosity caused by an increase in volume fraction could be the cause of this profile/behavior (Figs. 10–13). Table 1 shows that viscosity increases with an increase in volume fraction, hence an increase in the flow frictional losses. Apart from the dynamic viscosity, flow inertia, and boundary layer rupturing influences pressure drop [39].

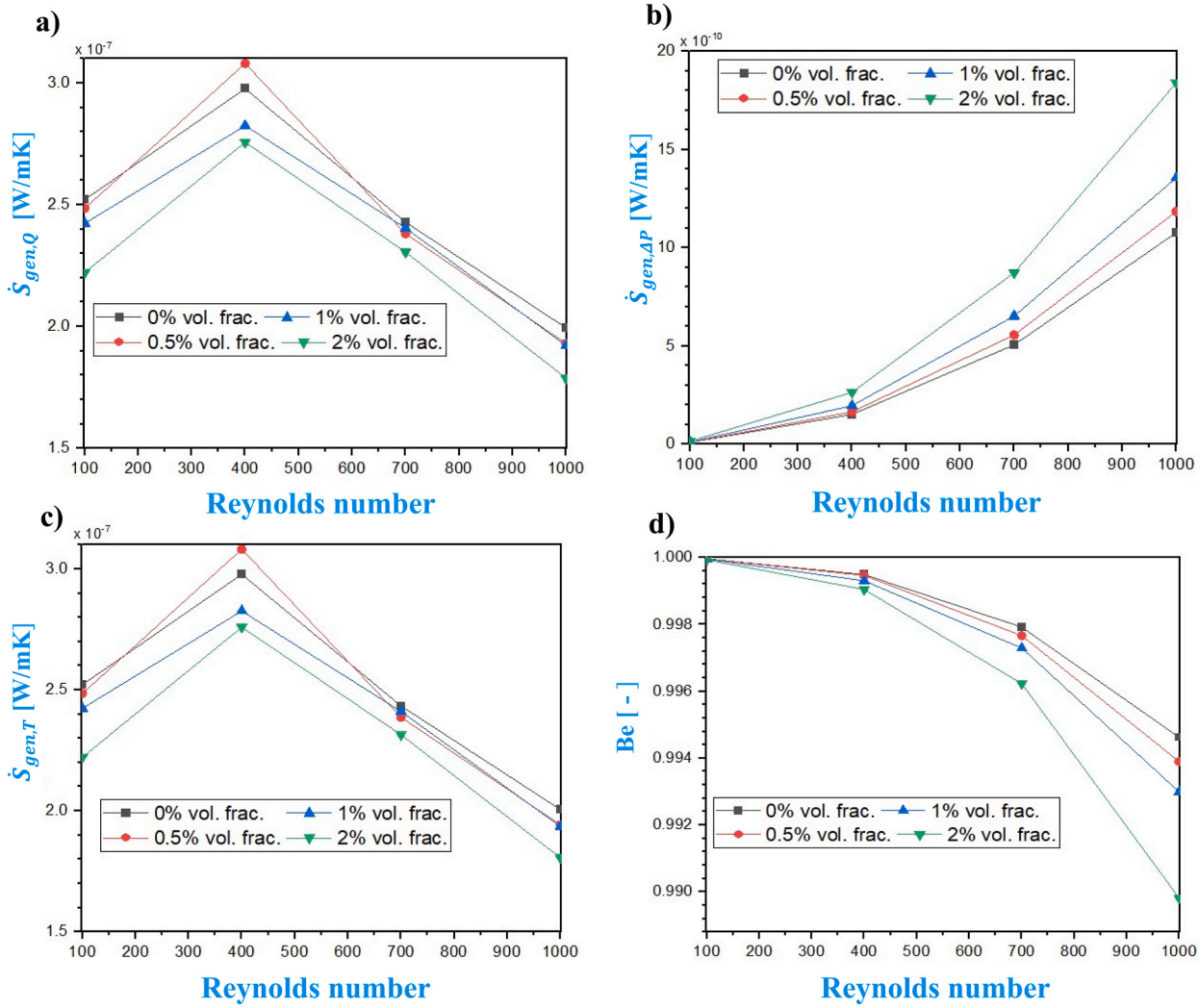

Fig. 23. Entropy production rates versus Reynolds number for a) heat transfer, b) pressure drop, c) total, and d) Bejan number for various nanofluid volume fractions for $\beta = -30.^{o}$

Moreover, a correlation occurs between the pressure drop and the Reynolds number, with the pressure drop increasing with the Reynolds number due to increased inertia force. In response to the inclination angle, the profile is sinusoidal in shape and the amplitude increases with Reynolds number.

In Figs. 10–12, it should be noted that for Re = 100–700, there is a slight drop in pressure as the inclination angle changes from -90° to -60°. This is due to the strong effect of gravitational force and momentum at -90° compared with the opposing frictional force. As the inclination angle changes, the gravitational force and momentum are reduced and the opposing frictional effect becomes significant until at the angle of -45° when the resultant force becomes maximum giving rise to the maximum pressure drop. As the inclination angle increases further from -45°, the forces due to gravity and momentum continue to reduce until at the horizontal orientation when the gravitational force effect is negligible. On the upward movement of the flow (against gravity), the gravitational force starts to become relevant (build-up), the frictional force changes direction and the momentum reduces because the flow is moving against gravity until at $\beta = +45^{\circ}$ when the maximum pressure drop is attained. Beyond this angle, the pressure drop due to fluid momentum continues to decrease and the resultant between the frictional and gravitational forces is reduced until $\beta = +90^{\circ}$. For Re = 1000, the effect of shear stress is large and the opposing frictional force causes a drastic reduction in the effective pressure drop at $\beta = 0^{\circ}$, and $\pm 90^{\circ}$ especially for higher volume fractions of 1.0% and 2.0% (Fig. 13). The maximum pressure drop is noted at the inclination angle of $\pm 45^{\circ}$. These trends were also reported by Uwadoka et al. [40].

5.3. *Entropy production rates: effects of tube inclination angle and volume fraction*

Entropy production rates are a measure of irreversibility in a thermal flow system. For an optimum design of a heat exchanger, it is

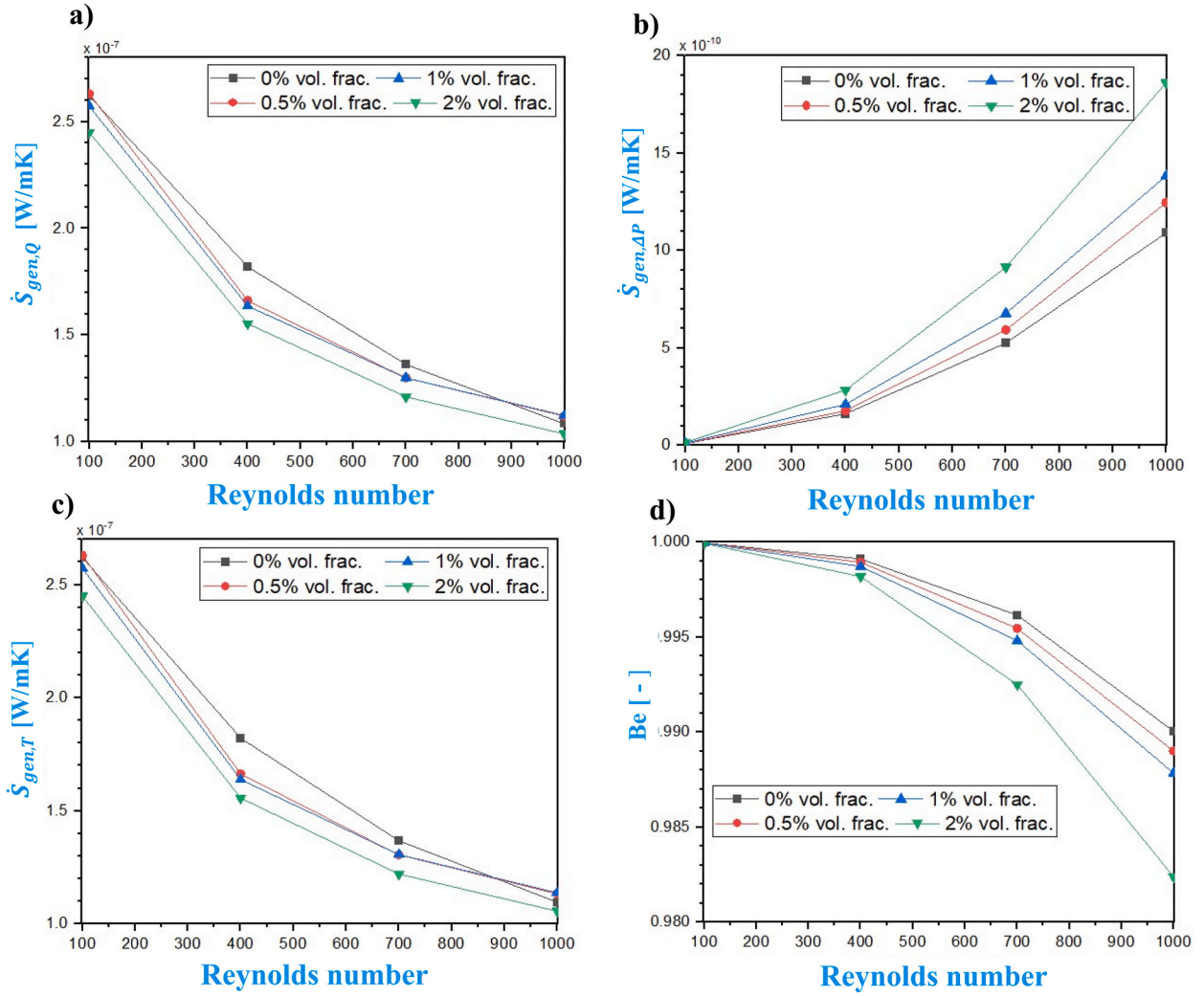

Fig. 24. Entropy production rates versus Reynolds number for a) heat transfer, b) pressure drop, c) total, and d) Bejan number for various nanofluid volume fractions for $\beta = -45.^{o}$

desired that the level of irreversibility is small. This section and the next will focus on the effects of inclination angle (i.e. gravitational force), volume fraction, and Reynolds number on the entropy production rates for the evaluation of a bionanofluid heat exchange system.

Figs. 14–17 display the results of the entropy production rates as a function of inclination angle for various volume fractions and Reynolds numbers. The thermal contributions to the total entropy production $\dot{S}_{gen,Q}$ dominates the flow, and it is a lot greater than the $\dot{S}_{gen,\Delta P}$. The figures of thermally induced entropy, $\dot{S}_{gen,Q}$, against inclination angle generally indicate an inverse correlation between the volume fraction and $\dot{S}_{gen,Q}$; that is, the larger the volume fraction, the lesser the $\dot{S}_{gen,Q}$, with a few exceptions (Figs. 14a–17a). For all Re, the trend for $\dot{S}_{gen,Q}$ and $\dot{S}_{gen,T}$ are similar and show oscillatory profiles with respect to the inclination angle because of the dominance of the heat transfer entropy production over the frictional component. For Re = 100, the minimum values are seen at the angles of -30° and $+60^{\circ}$, while the maximum is observed for horizontal and vertical orientations (0° and $\pm 90^{\circ}$). For Re > 100, the minimum values occur at the inclination angles of $\pm 45^{\circ}$, while the maximum values are still observed for horizontal and vertical orientations. This trend can be attributed to the large difference between the fluid bulk and the wall temperature during the horizontal and vertical tube orientations and the impact of the gravitational field and other forces interplaying during the flow.

The values of $\dot{S}_{gen,\Delta P}$, in contrast to that of $\dot{S}_{gen,Q}$, increases with respect to the volume fraction (Figs. 14b–17b). For Re = 100, for each volume fraction and inclination angle, the $S_{gen,\ \Delta P}$, displays a relatively smaller variation compared with the thermal contribution. For Re = 400, the same relationship holds, except for the abrupt drop in the $\dot{S}_{gen,\Delta P}$ for $\beta = 0^{\circ}$ (horizontal orientation), when $\varphi = 1.0\%$. This trend was noted by Chinakwe et al. [41] and was attributed to a large temperature difference between the wall and the bulk fluid as the inclination angle changes from horizontal to upward or downward flow. For Re of 700 and 1000, the variations in $\dot{S}_{gen,\Delta P}$

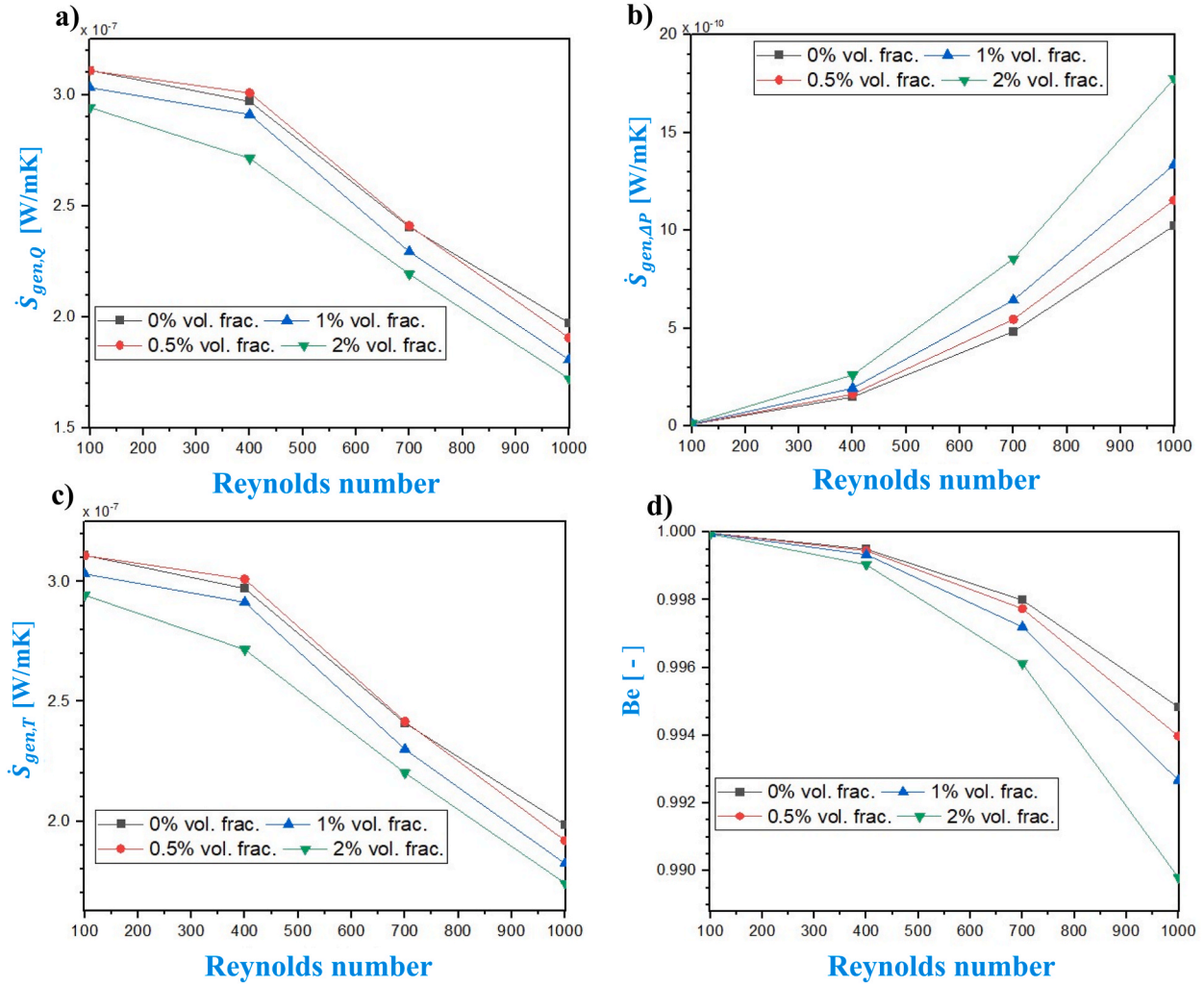

Fig. 25. Entropy production rates versus Reynolds number for a) heat transfer, b) pressure drop, c) total, and d) Bejan number for various nanofluid volume fractions for $\beta = -60.^{o}$

increases and are maximum for $\beta = \pm 45°$.

The Bejan number and volume fraction appear to have an inverse correlation, meaning that as the volume fraction rises, the Bejan number decreases (Figs. 14d–17d). For Re = 100, the minimum Bejan numbers are obtained at the inclination angles of $-30°$ and $+60°$, while the maximum corresponds to the horizontal and vertical (Fig. 14d). For Re = 400–1000, the minimum Began number corresponds to $\beta = \pm 45°$ for $\varphi = 2.0\%$ vol. while the maximum occurs for $\varphi = 1.0\%$ vol. for Re = 400 and $\varphi = 0.5\%$ vol. for Re = 1000. Furthermore, the Bejan number tends to decrease as the Reynolds number rises. This could be attributed to the increased shear hence, frictional entropy production.

In summary, irreversibility varies with inclination angle, Reynolds number, and volume fraction, and it is minimal at the inclination angle of $-30°$ and $+60°$ for Re = 100 and $\pm 45°$ for Re > 100. It, therefore, implies that the optimum operational performance of the system can be obtained at these tube orientations. There are other studies on the influence of inclination angle (i.e. gravitational force) on entropy production rates [41,42].

5.4. *Entropy production rates: effects of Reynolds number and volume fraction*

The results of the entropy production rates with regard to the Reynolds number are shown in Figs. 18–26 for various inclination angles. The $\dot{S}_{gen,Q}$ and $\dot{S}_{gen,T}$ show a monotonically decreasing trend with Reynolds number while the converse is displayed by $\dot{S}_{gen,\Delta P}$. However, there are a few cases when the trends are at variance. For example, for inclination angles of $-30°$ and $+60°$, in Figs. 20 and 23, there is an increase in the $\dot{S}_{gen,Q}$ and $\dot{S}_{gen,T}$ as the flow transits from Re = 100–400, after which there is a fall as Re continues to increase. This could be because of the small temperature difference noted for Re = 100 at these orientations. For these cases, the heat transfer coefficients are significantly high (Fig. 6). Also, for the inclination angle of $+90°$ (Fig. 21), the volume fraction of 0.0%, the

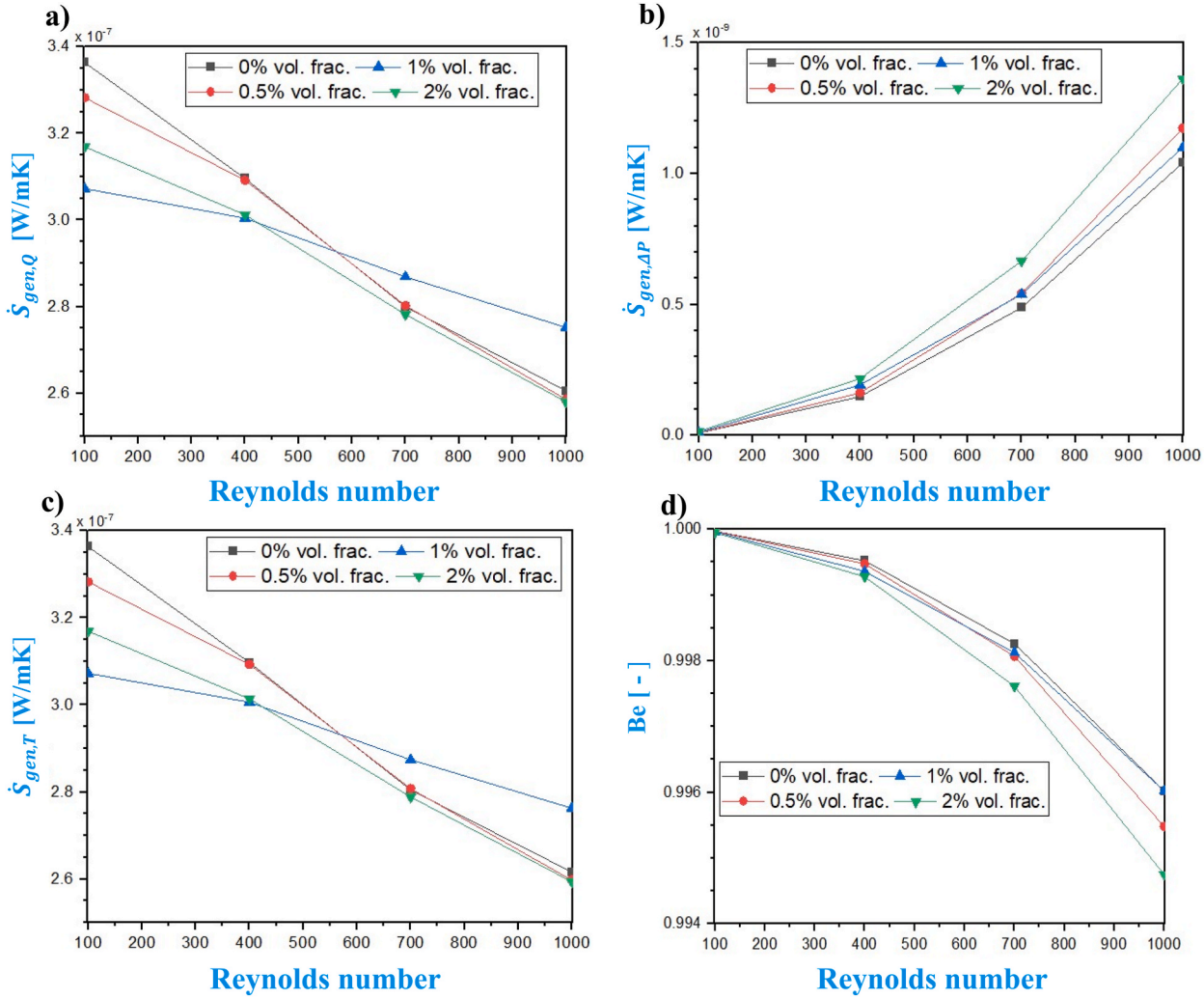

Fig. 26. Entropy production rates versus Reynolds number for a) heat transfer, b) pressure drop, c) total, and d) Bejan number for various nanofluid volume fractions for $\beta = -90.^{o}$

heat transfer contribution to and total entropy production increases as Reynolds number increases from 100 to 400 before reducing while for φ = 0.5–2.0% vol. there is a downward trend as Re increases. For horizontal tube orientations, there is a sharp rise in the heat transfer contribution and a notable decrease in the frictional pressure contribution for φ = 1.0% vol (Fig. 22). resulting in a noticeable change in the total entropy production and Bejan number.

5.5. *Temperature variation contours at the exit region*

Fig. 27 shows the profile of the flow's total static temperature with respect to the inclination angle for Re = 100 and volume fraction of 2.0% vol. at the exit region (downstream) of the tube. The effect of gravitational force on the thermal boundary layer can be seen in the heat transfer coefficient in Fig. 6 as discussed in section 5.1. It shows that inclination angles of 0°, and ±90° have a low heat transfer coefficient. While the effect of gravitational force is minimal on the flow for β = 0°, it is maximum on the flow for β = ±90°. It therefore implies that for β = 0°, the gravitational effect is minimal and the thermal boundary layer is impacted only by the frictional force hence, the difference between the bulk and wall temperature is large resulting in a significant bulk temperature (Fig. 27e). For β = +30°, the effect of gravity is only increased a little and does not change the bulk temperature significantly from when β = 0° (Fig. 27d). For other flow configurations, the temperature difference between the bulk and wall, hence the bulk temperature is small due to the gravitational effect on the thermal boundary layer.

6. Conclusion

The influence of the gravitational force (in terms of inclination angle), Reynolds number, and volume fraction of the bionanofluid

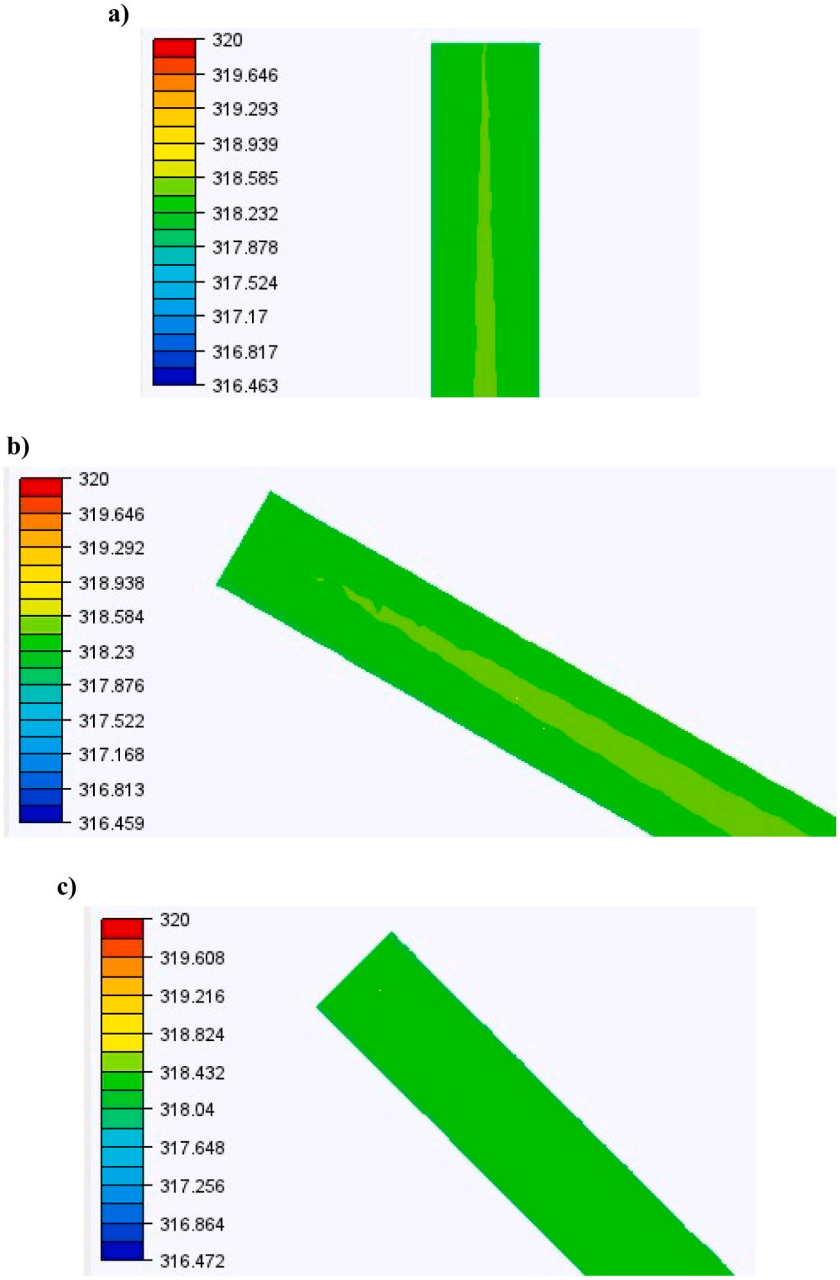

Fig. 27. Temperature variation at outlet for Re = 100, φ = 2.0% and β = a) +90°, b) +60°, c) +45°, d) +30°, e) 0°, f) −30°, g) −45°, h) −60°, i) −90 °

on the heat transfer coefficient, pressure drop, and rates of entropy production in inclined tubes are investigated for the flow of the mango bark/CO_2 nanofluid in a tube with constant heat flux. Using Reynolds numbers ranging from 100 to 1000, inclined tube flows of 0°, ±30°, ±45°, ±60°, and ±90°, and volume fractions of 0.0%, 0.5%, 1.0%, and 2.0% vol., the findings show that gravitational force along with other forces that interplay in the in-tube flow of bionanofluids impacts on the thermal boundary layer and can significantly reduce or increase the temperature difference between the bulk fluid and wall. The study variables have been found to significantly influence the thermal, hydraulic, and irreversibility parameters of a bionanofluid flow. The following are the key findings of the study:

1). the optimal tube inclination angle that produces the highest heat transfer coefficients are −30° and +60° for Re = 100 and ± 45° for Re > 100. These correspond to the nanofluid volume fraction of 2.0% vol. At these inclination angles, the thermal

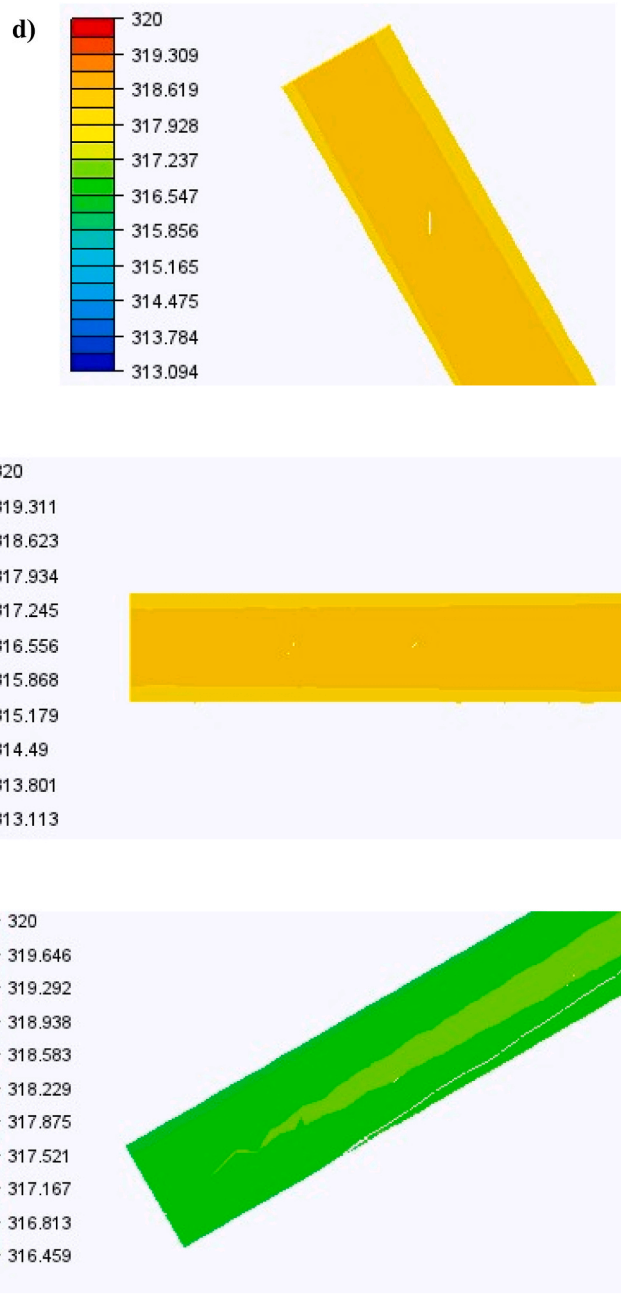

Fig. 27. (*continued*).

enhancements due to the gravity effect are 42.0%, 93.4%, 121.3%, and 150.0% for Reynolds numbers of 100, 400, 700, and 1000, respectively, while the nanoparticles give less than 16.0%.

2). maximum pressure drops correspond to $\pm 45^{\circ}$ for the volume fraction of 2.0% vol. meaning that the pressure penalty is highest at these inclination angles.

3). while the heat transfer contribution to the total entropy production decreases with nanofluid volume fraction, the converse is the frictional pressure drop contribution.

4). the minimum total entropy production rates which correspond to minimum irreversibilities are obtained for the volume fraction of 2.0%. They occur at the inclination angles of -30° and $+60^{\circ}$ for $Re = 100$ and $\pm\ 45^{\circ}$ for $Re > 100$.

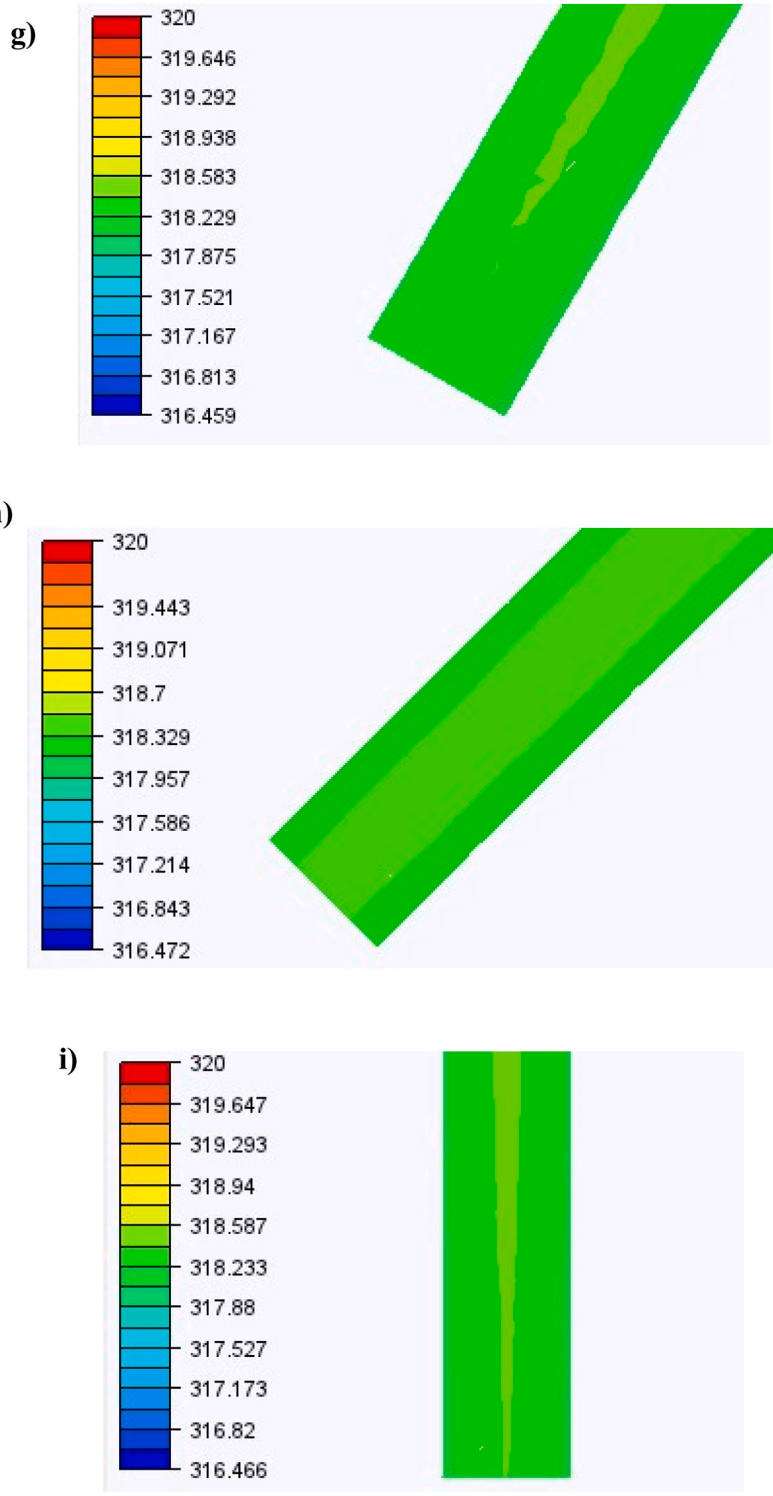

Fig. 27. (*continued*).

Author contribution statement

Okwesilieze Uwadoka: Performed the experiments; Wrote the paper.
Adekunle Adelaja: Conceived and designed the experiments; Contributed reagents, materials, analysis tools or data; Wrote the

paper.

Olabode Olakoyejo; Opeyemi Fadipe; Steven Efe: Analyzed and interpreted the data; Contributed reagents, materials, analysis tools or data.

Data availability statement

Data will be made available on request.

Declaration of competing interest

The authors declare that they have no known competing financial interests or personal relationships that could have appeared to influence the work reported in this paper

Acknowledgment

Public, private, or nonprofit funding organizations did not provide any grants for this particular study.

References

[1] W.H. Azmi, M.Z. Sharif, T.M. Yusof, R. Mamat, A.A.M. Redhwan, Potential of nanorefrigerant and nanolubricant on energy saving in refrigeration system - a review, Renew. Sustain. Energy Rev. (2017) 415–428.
[2] G. Lorentzen, J. Pettersen, A new, efficient and environmentally benign system for car air-conditioning, Int. J. Refrig. 16 (1) (1993) 4–12, https://doi.org/10.1016/0140-7007(93)90014-Y.
[3] E. Groll, J.-H. Kim, Review article: review of recent advances toward transcritical CO_2 cycle technology, HVAC R Res. 13 (3) (2007) 499–520, https://doi.org/10.1080/10789669.2007.10390968.
[4] C.-H. Son, H.-K. Oh, Condensation heat transfer characteristics of CO2 in a horizontal smooth- and microfin-tube at high saturation temperatures, Appl. Therm. Eng. 36 (2012) 51–62, https://doi.org/10.1016/j.applthermaleng.2011.12.017.
[5] T.O. Babarinde, S.A. Akinlabi, D.M. Madyira, Enhancing the performance of vapour compression refrigeration system using nano refrigerants: a review, IOP Conf. Ser. Mater. Sci. Eng. 413 (2018), 012068, https://doi.org/10.1088/1757-899X/413/1/012068.
[6] M. Yari, Exergetic analysis of the vapour compression refrigeration cycle using ejector as an expander, Int. J. Exergy 5 (3) (2008) 326, https://doi.org/10.1504/IJEX.2008.018114.
[7] Nasiruddin, M.H.K. Siddiqui, Heat transfer augmentation in a heat exchanger tube using a baffle, Int. J. Heat Fluid Flow 28 (2) (2007) 318–328, https://doi.org/10.1016/j.ijheatfluidflow.2006.03.020.
[8] S.U.S. Choi, J.A. Eastman, Enhancing thermal conductivity of fluids with nanoparticles, in: International mechanical engineering congress and exhibition, 1995, pp. 12–17.
[9] O. Uwadoka, A.O. Adelaja, O.O. Noah, O.L. Fadipe, S.W. Lee, Numerical investigation of heat transfer and pressure drop characteristics of mango bark-CO2 nanofluid in inclined gas cooling process, Closing Carbon Cycles – A Transformation Process Involving Technology, Economy, and Society: Part I, Energy 26 (2022) 2004–2965, https://doi.org/10.46855/energy-proceedings-10139.
[10] R. Senthilkumar, S. Vaidyanathan, B. Sivaraman, Effect of inclination angle in heat pipe performance using copper nanofluid, Procedia Eng. 38 (2012) 3715–3721, https://doi.org/10.1016/j.proeng.2012.06.427.
[11] M. Akbari, A. Behzadmehr, F. Shahraki, Fully developed mixed convection in horizontal and inclined tubes with uniform heat flux using nanofluid, Int. J. Heat Fluid Flow 29 (2) (2008) 545–556, https://doi.org/10.1016/j.ijheatfluidflow.2007.11.006.
[12] A. Karimipour, M. Hemmat Esfe, M.R. Safaei, D. Toghraie Semiromi, S. Jafari, S.N. Kazi, Mixed convection of copper–water nanofluid in a shallow inclined lid driven cavity using the lattice Boltzmann method, Phys. Stat. Mech. Appl. 402 (2014) 150–168, https://doi.org/10.1016/j.physa.2014.01.057.
[13] M. Izadi, A. Behzadmehr, M.M. Shahmardan, Effects of inclination angle on mixed convection heat transfer of a nanofluid in a square cavity, Int. J. Comput. Methods Eng. Sci. Mech. 16 (1) (2015) 11–21, https://doi.org/10.1080/15502287.2014.976674.
[14] R. ben Mansour, N. Galanis, C.T. Nguyen, Experimental study of mixed convection with water–Al_2O_3 nanofluid in inclined tube with uniform wall heat flux, Int. J. Therm. Sci. 50 (3) (2011) 403–410, https://doi.org/10.1016/j.ijthermalsci.2010.03.016.
[15] Z.-H. Liu, Y.-Y. Li, R. Bao, Thermal performance of inclined grooved heat pipes using nanofluids, Int. J. Therm. Sci. 49 (9) (2010) 1680–1687, https://doi.org/10.1016/j.ijthermalsci.2010.03.006.
[16] A.K. Reji, G. Kumaresan, A. Sarathi, A.G.P. Saiganesh, R. Suriya Kumar, M.M. Shelton, Performance analysis of thermosyphon heat pipe using aluminum oxide nanofluid under various angles of inclination, Mater. Today Proc. 45 (2021) 1211–1216, https://doi.org/10.1016/j.matpr.2020.04.247.
[17] W.I.A. Aly, M.A. Elbalshouny, H.M. Abd El-Hameed, M. Fatouh, Thermal performance evaluation of a helically-micro-grooved heat pipe working with water and aqueous Al_2O_3 nanofluid at different inclination angle and filling ratio, Appl. Therm. Eng. 110 (2017) 1294–1304, https://doi.org/10.1016/j.applthermaleng.2016.08.130.
[18] K. Bartelt, Y. Park, L. Liu, A. Jacobi, Y.-G. Park, A.M. Jacobi, Flow-boiling of R-134a/CuO nanofluids in a horizontal tube [Online]. Available: http://docs.lib.purdue.edu/iracc/928, 2008.
[19] K. Henderson, Y.-G. Park, L. Liu, A.M. Jacobi, Flow-boiling heat transfer of R-134a-based nanofluids in a horizontal tube, Int. J. Heat Mass Tran. 53 (5–6) (2010) 944–951, https://doi.org/10.1016/j.ijheatmasstransfer.2009.11.026.
[20] W.H. Mah, Y.M. Hung, N. Guo, Entropy generation of viscous dissipative nanofluid flow in microchannels, Int. J. Heat Mass Tran. 55 (15–16) (2012) 4169–4182, https://doi.org/10.1016/j.ijheatmasstransfer.2012.03.058.
[21] M. Moghaddami, A. Mohammadzade, S.A.V. Esfehani, Second law analysis of nanofluid flow, Energy Convers. Manag. 52 (2) (2011) 1397–1405, https://doi.org/10.1016/j.enconman.2010.10.002.
[22] J. Li, C. Kleinstreuer, Entropy generation analysis for nanofluid flow in microchannels, J. Heat Tran. 132 (12) (2010), https://doi.org/10.1115/1.4002395.
[23] A. Ebrahimi, F. Rikhtegar, A. Sabaghan, E. Roohi, Heat transfer and entropy generation in a microchannel with longitudinal vortex generators using nanofluids, Energy 101 (2016) 190–201, https://doi.org/10.1016/j.energy.2016.01.102.
[24] S. Heshmatian, M. Bahiraei, Numerical investigation of entropy generation to predict irreversibilities in nanofluid flow within a microchannel: effects of Brownian diffusion, shear rate and viscosity gradient, Chem. Eng. Sci. 172 (2017) 52–65, https://doi.org/10.1016/j.ces.2017.06.024.
[25] Y.-T. Yang, Y.-H. Wang, B.-Y. Huang, Numerical optimization for nanofluid flow in microchannels using entropy generation minimization, Num. Heat Transf. A Appl. 67 (5) (2015) 571–588, https://doi.org/10.1080/10407782.2014.937282.
[26] S.K. Mohammadian, H. Reza Seyf, Y. Zhang, Performance augmentation and optimization of aluminum oxide-water nanofluid flow in a two-fluid microchannel heat exchanger, J. Heat Tran. 136 (2) (2014), https://doi.org/10.1115/1.4025431.
[27] M.R. Sohel, R. Saidur, N.H. Hassan, M.M. Elias, S.S. Khaleduzzaman, I.M. Mahbubul, Analysis of entropy generation using nanofluid flow through the circular microchannel and minichannel heat sink, Int. Commun. Heat Mass Tran. 46 (2013) 85–91, https://doi.org/10.1016/j.icheatmasstransfer.2013.05.011.

[28] S. Kakaç, A. Pramuanjaroenkij, Review of convective heat transfer enhancement with nanofluids, Int. J. Heat Mass Tran. 52 (13–14) (2009) 3187–3196, https://doi.org/10.1016/j.ijheatmasstransfer.2009.02.006.
[29] R.K. Shah, Thermal entry length solutions for the circular tube and parallel plates, in: Proceedings of 3rd National Heat and Mass Transfer Conference, 1975, pp. 11–75.
[30] D. Wen, Y. Ding, Experimental investigation into convective heat transfer of nanofluids at the entrance region under laminar flow conditions, Int. J. Heat Mass Tran. 47 (24) (2004) 5181–5188, https://doi.org/10.1016/j.ijheatmasstransfer.2004.07.012.
[31] S.Z. Heris, S. Gh Etemad, M.N. Esfahany, Convective heat transfer of a Cu/water nanofluid flowing through a circular tube, Exp. Heat Tran. 22 (4) (2009) 217–227, https://doi.org/10.1080/08916150902950145.
[32] E. Nourafkan, G. Karimi, J. Moradgholi, Experimental study of laminar convective heat transfer and pressure drop of cuprous oxide/water nanofluid inside a circular tube, Exp. Heat Tran. 28 (1) (2015) 58–68, https://doi.org/10.1080/08916152.2013.803178.
[33] E.J. Onyiriuka, A.I. Obanor, M. Mahdavi, D.R.E. Ewim, Evaluation of single-phase, discrete, mixture and combined model of discrete and mixture phases in predicting nanofluid heat transfer characteristics for laminar and turbulent flow regimes, Adv. Powder Technol. 29 (11) (2018) 2644–2657, https://doi.org/10.1016/j.apt.2018.07.013.
[34] E.J. Onyiriuka, O.O. Ighodaro, A.O. Adelaja, D.R.E. Ewim, S. Bhattacharyya, A numerical investigation of the heat transfer characteristics of water-based mango bark nanofluid flowing in a double-pipe heat exchanger, Heliyon 5 (9) (2019), e02416, https://doi.org/10.1016/j.heliyon.2019.e02416.
[35] O.S. Omosehin, A.O. Adelaja, O.T. Olakoyejo, O. Oluwatusin, M.O. Oyekeye, S.M. Abolarin, Numerical study of the thermal-hydraulic performance of water-based Al_2O_3 - Cu hybrid nanofluids in a double-layer microchannel heat sink, Closing Carbon Cycles – A Transformation Process Involving Technology, Economy, and Society: Part I, Energy 26 (2022) 2004–2965, https://doi.org/10.46855/energy-proceedings-10142.
[36] O.S. Omosehin, A.O. Adelaja, O.T. Olakoyejo, M.O. Oyekeye, Numerical study of the thermal performance and pressure drops of water-based Al_2O_3 - Cu hybrid nanofluids of different compositions in a microchannel heat sink, Microfluid. Nanofluidics 26 (7) (2022) 49, https://doi.org/10.1007/s10404-022-02550-2.
[37] C. Sasmal, Analysis of the effects of inclination angle, nanoparticle volume fraction and its size on forced convection from an inclined elliptic cylinder in aqueous nanofluids, J. Therm. Anal. Calorim. 136 (3) (2018) 1433–1445, https://doi.org/10.1007/s10973-018-7750-5.
[38] Y. Wu, Z. Zhang, W. Li, D. Xu, Effect of the inclination angle on the steady-state heat transfer performance of a thermosyphon, Appl. Sci. 9 (16) (2019) 3324, https://doi.org/10.3390/app9163324.
[39] V. Kumar, J. Sarkar, Numerical and experimental investigations on heat transfer and pressure drop characteristics of Al_2O_3-TiO_2 hybrid nanofluid in minichannel heat Sink with different mixture ratio, Powder Technol. 345 (2019) 717–727, https://doi.org/10.1016/j.apt.2019.11.017.
[40] O. Uwadoka, A.O. Adelaja, O.T. Olakoyejo, O.L. Fadipe, S. Efe, Effect of inclination angle on the laminar flow of CO_2-mango bark nanofluid in inclined tube-in-tube heat exchanger, Urban Energy Systems towards Carbon Neutrality, Energy Proc. (2023) 1–7, https://doi.org/10.46855/energy-proceedings-10333.
[41] C. Chinakwe, A. Adelaja, M. Akinseloyin, O.T. Olakoyejo, Effect of inclination angle on the thermal-hydraulic characteristics and entropy generation of Al2O3–water nanofluid for in-tube turbulent flow, World J. Eng. (2023), https://doi.org/10.1108/WJE-12-2022-0487.
[42] A.O. Adelaja, J. Dirker, J.P. Meyer, Experimental study of entropy generation during condensation in inclined enhanced tubes, Int. J. Multiphas. Flow 145 (2021), 103841, https://doi.org/10.1016/j.ijmultiphaseflow.2021.103841.